

Implication of the dark axion portal for the EDM of fermions and dark matter probing with NA64e, NA64 μ , LDMX, M³, and BaBar.

Alexey S. Zhevlakov,^{1,2} Dmitry V. Kirpichnikov,³ and Valery E. Lyubovitskij^{4,5,6,7,8}

¹*Bogoliubov Laboratory of Theoretical Physics, JINR, 141980 Dubna, Russia*

²*Matrosov Institute for System Dynamics and Control Theory SB RAS Lermontov str., 134, 664033, Irkutsk, Russia*

³*Institute for Nuclear Research of the Russian Academy of Sciences, 117312 Moscow, Russia*

⁴*Institut für Theoretische Physik, Universität Tübingen,*

Kepler Center for Astro and Particle Physics, Auf der Morgenstelle 14, D-72076 Tübingen, Germany

⁵*Departamento de Física y Centro Científico Tecnológico de Valparaíso-CCTVal,*

Universidad Técnica Federico Santa María, Casilla 110-V, Valparaíso, Chile

⁶*Millennium Institute for Subatomic Physics at the High-Energy Frontier (SAPHIR) of ANID, Fernández Concha 700, Santiago, Chile*

⁷*Department of Physics, Tomsk State University, 634050 Tomsk, Russia*

⁸*Tomsk Polytechnic University, 634050 Tomsk, Russia*

(Dated: April 22, 2022)

The link between ordinary Standard model (SM) photon and both dark photon and axion like particle (ALP) can be introduced through the dark axion portal coupling. Given the dark axion portal setup, in the present paper we refer the dark photon as the mediator between SM and dark matter (DM) particles, implying that it decays predominantly into pair of DM fermions. Furthermore, we discuss in detail the implication of the dark axion portal scenario for the lepton (electron and muon) fixed target experiments. In particular, for the specific fixed target facility we study the missing energy signatures of the dark photon production followed by its invisible decay into stable DM particles. We investigated the potential to probe dark axion portal vertices with regarding signatures and derive the expected sensitivities of NA64e, NA64 μ , LDMX and M³. Moreover, we estimated the expected reach of NA64e from the projected statistics of the J/ψ vector meson invisible decays. We also recasted BaBar monophoton bounds for the specific dark axion portal scenario. In addition, we modified the dark axion portal setup by including in the model both the hadron and lepton specific ALP couplings. As the result, we obtain the bounds on the combination of fermion-specific couplings of ALP from the fixed target experiments. We discuss the implication of the modified dark axion portal scenario for the electric dipole moments (EDM) of SM fermions. In addition, we derived the novel constraints on the combination of the CP -violating neutron-specific ALP couplings from the existing bounds on neutron EDM by taking into account the neutron anomalous magnetic moment.

I. INTRODUCTION

Axion and axion like particles (ALPs) arise naturally in the Standard Model (SM) extensions which are connected with CP -violation problem in strong interaction physics [1, 2], can explain muon ($g-2$) anomaly [3, 4] and Dark Matter (DM) abundance [5–7]. A more exotic cases of ALPs phenomenology that include a lepton flavor violation effects are studied in the literature thoroughly [8–11]. The ALPs and other dark sector particles have been extensively discussed recently in context of the experimental searches (see, e. g., Refs. [12–37] and references therein).

The link between SM and dark sector particles can be established through the idea of *portal* [38]. For instance, that concept includes such scenarios as the Higgs portal [39], the dark photon portal [40–42], sterile neutrino portal [43] and axion portal [44]. These portals offer systematic examination of the DM and also give rise to novel experimental signatures.

Recently, a new *dark axion portal* was suggested [45, 46] to provide the dark photon production mechanism in the early Universe, implying the explanation of DM abundance due to the sufficiently light dark photon. Such

portal connects the axion or ALPs and dark photon via both axion–SM photon–dark photon and axion–dark photon–dark photon couplings.

Now let us briefly summarize recent progress in the dark axion portal. In particular, an authors of Ref. [47] have developed the idea of dark axion portal in order to explain the DM cosmic density through the mixture of both axions and dark photons. In addition, in Ref. [48] authors discussed in detail the implication of the relevant portal for the leptonic ($g-2$) anomalies, B-factories, fixed target neutrino experiments and beam dumps. Also there has been previous study [49] of the monophoton signal for the future experiments SHIP [50] and FASER [51] in the framework of dark axion portal. Moreover, the detailed analysis of the regarding monophoton signatures and the expected sensitivities of reactor neutrino experiments was presented in Ref. [52]. An authors of Ref. [53] suggested the scenario that provides a novel link between the phenomenological dark axion portal, dark photons, and the hierarchy problem of the Higgs mass. In addition, the Ref. [54] proposed a new scenario of using the dark axion portal at one-loop level in order to explain recent result of the Fermilab Muon ($g-2$) experiment on the muon anomalous magnetic moment.

In the first part of this paper we develop the ideas presented in Refs. [55, 56] where the implication of light sub-GeV bosons for electric dipole moments (EDM) of fermions and CP -odd dark axion portal coupling was discussed in detail. In particular, we study the contribution of CP -violation vertices of SM fermions and ALPs to EDM and derive novel constraint on combination of couplings of neutron with ALPs. In addition, we argue that the EDM of fermions can be induced by: (i) CP -odd Yukawa-like couplings of ALP, (ii) CP -even interaction of SM fermions and dark photon and (iii) CP -even dark axion portal coupling. As a result, one can obtain the bounds on the combination of regarding couplings.

The second part of the paper develops the idea suggested in Ref. [48, 49] that implies the probing the dark ALP portal scenario through the dark photon decaying predominantly to the DM particles. In this setup it is assumed that dark photon is the gauge field of the hidden $U_D(1)$ group and thus it can serve the mediator between DM and SM particles via dark axion portal interaction. We show that regarding scenario has a very broad phenomenological implication and can be probed via missing energy signatures in the existed, NA64e [31–35] and NA64 μ [57–60], and the projected, LDMX [61–66] and M³ [67, 68], lepton fixed target facilities. We also recast the BaBar constraints on the dark ALP portal scenario with dark photon decaying mainly to DM fermion pair. In addition we address to CP -violating interaction of ALP with SM fermions in order to modify dark ALP portal scenario, as a result we obtain the expected bounds on the combination of hadron-specific and lepton-specific couplings from NA64e, NA64 μ , LDMX and M³.

The paper is organized as follows. In Sec. II we provide the description of the considered modified dark ALP portal scenarios. In Sec. III we consider dark ALP portal applied to generation of EDM. In Sec. IV we give a description of the missing energy signatures for the analysis of dark matter production at the fixed target experiments. In Sec. V we show that dark ALP portal couplings can be constrained by using the data from e^+e^- colliders and the experiments that exploit the electron and muon beam impinging on the fixed target. In Sec. VI and Sec. VII we obtain the constraints on combination of dark axion portal coupling with both hadron-specific and lepton-specific interactions, respectively. In Sec. VIII we summarize our main results.

II. THE DESCRIPTION OF THE BENCHMARK SCENARIOS

One of the possible connection between SM and dark sector particles is vector portal via the coupling of the SM and dark photons. One can describe this mixing by using the effective phenomenological Lagrangian

$$\mathcal{L}_{\text{vector portal}} = \frac{\epsilon}{2} F_{\mu\nu} F'^{\mu\nu}, \quad (1)$$

where ϵ is the kinetic mixing parameter between the two $U(1)$ gauge symmetries [69], $F_{\mu\nu}$ and $F'_{\mu\nu}$ are the strength tensors of SM electromagnetic and DM dark gauge (dark photon) fields, respectively. Nevertheless, in the present analysis we assume throughout the paper that $\epsilon \ll 1$, implying complete neglecting the vector portal mixing in Eq. (1).

In what follows, one can assume [45, 46] that mixing between dark and electromagnetic photons can be associated with ALPs interaction. The effective Lagrangian for such nonrenormalizable dark axion portal has form

$$\mathcal{L}_{\text{dark axion portal}} = \frac{g_{a\gamma D\gamma D}}{4} a F'_{\mu\nu} \tilde{F}'^{\mu\nu} + \frac{g_{a\gamma\gamma D}}{2} a F_{\mu\nu} \tilde{F}'^{\mu\nu}, \quad (2)$$

where the first term is the coupling between ALP and two dark photons, the second terms is the interaction between ALP and both SM and dark photon.

First, we consider the benchmark extension of the dark axion portal setup by exploiting the dark matter (DM) Lagrangian, such that the dark photon serves the mediator between visible SM photon and hidden DM sector through the Lagrangian Eq. (2). In particular, we specify throughout the paper the Lagrangian

$$\mathcal{L} \supset \mathcal{L}_{\text{dark axion portal}} + \bar{\chi}(\gamma^\mu i\partial_\mu - g_D \gamma^\mu A'_\mu + m_\chi)\chi, \quad (3)$$

that is referred to

- *the minimal dark ALP portal scenario.*

The field χ in Eq. (3) is a Dirac DM fermion of mass m_χ from the dark sector, g_D is the coupling constant between DM and dark photon A'_μ field, that is associated with hidden charge of the $U_D(1)$ gauge group. Moreover, we assume that dark photon decays predominantly to dark fermion $\chi\bar{\chi}$ pair.

Second, we also employ a simplified model framework, with CP -violation Yukawa coupling between ALP and SM fermions than can be written as:

$$\mathcal{L} \supset \mathcal{L}_{\text{dark axion portal}} + \bar{\chi}(\gamma^\mu i\partial_\mu - g_D \gamma^\mu A'_\mu + m_\chi)\chi + \sum_\psi a \bar{\psi}(g_\psi^s + i g_\psi^p \gamma_5)\psi, \quad (4)$$

where the couplings, g_ψ^s and g_ψ^a , are restricted to be from two benchmark scenarios

- *the non-minimal lepton-specific ALP setup:* $g_\psi^s \neq 0$, $g_\psi^p \neq 0$ for $\psi = e, \mu$, where e and μ are electron and muon respectively, and $g_\psi^s = g_\psi^p = 0$ for $\psi = n, p$, where p and n are proton and neutron respectively;
- *the non-minimal hadron-specific ALP setup:* $g_\psi^s \neq 0$, $g_\psi^p \neq 0$ for $\psi = n, p$ and $g_\psi^s = g_\psi^p = 0$ for $\psi = e, \mu$.

The Yukawa-like couplings of the Lagrangian (4) may originate from an effective interaction [70–73] in framework of the two-Higgs-doublet-model. Moreover

since such terms violate the CP symmetry, thus they can induce the electric dipole moment (EDM) [74, 75] of fermions. It is worth to estimate the bounds on the regarding couplings from the EDM of fermions in the framework of both the lepton-specific and hadron-specific scenarios. That study is of particular interest of the present paper. In Sec III we discuss its phenomenological implication.

In addition, for the specific benchmark scenario one can obtain also the upper limit/expected sensitivity on either the coupling $g_{a\gamma\gamma_D}$ or the combination of couplings $|g_{a\gamma\gamma_D}g_\psi^s|$ and $|g_{a\gamma\gamma_D}g_\psi^p|$ from the null result of DM detection in the BaBar e^+e^- collider and in the fixed target experiments such as NA64 $e(\mu)$ at CERN SPS and LDMX, M³ at FermiLab. We discuss that in detail in Secs. IV, V, VI, and VII.

III. EDM

Let us consider the bounds on ALPs couplings from the experimental constraints on EDM fermions (electron, muon, and neutron) generated by CP -violating Lagrangian [76, 77]. We can estimate a contribution to EDM by calculation a simple Feynman diagrams (see Fig. 1) with intermediate ALP exchange [55]. The contribution to fermion EDM with mass m_ψ has a form:

$$d_\psi = \frac{eg_\psi^s g_\psi^p}{8\pi^2 m_\psi} g_i(y) \quad (5)$$

where index $i = 1$ labels the lepton couplings ($\psi = e, \mu$) with the function $g_1(y)$ being

$$g_1(y) = \int_0^1 dx \frac{x^2}{x^2 + y^2(1-x)}, \quad (6)$$

here $y = m_a/m_\psi$. For neutron case ($\psi = n$) we specify the index $i = 2$ in Eq. (5). Then one should account the neutron interaction with external electromagnetic field A_μ through the anomalous magnetic moment (see diagrams on Fig.2). The regarding Lagrangian can be written in the following form

$$\mathcal{L}_{ANN} = ieA_\mu \bar{N} \left(\gamma^\mu Q_N + \frac{i\sigma^{\mu\nu} q_\nu}{2m_N} k_N \right) N, \quad (7)$$

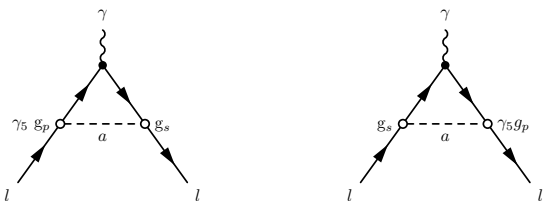


FIG. 1. Feynman diagrams with taking into account ALPs which generate EDM of charge fermions, leptons.

where m_N is the nucleon mass, $Q_N = \text{diag}(1, 0)$ and $k_N = \text{diag}(k_p, k_n)$ are the matrices of the electric charges and anomalous magnetic moments of nucleons (proton p and neutron n), respectively, with $k_p = 1.793$ and $k_n = -1.913$. Here, $\sigma^{\mu\nu} = \frac{i}{2}[\gamma^\mu, \gamma^\nu]$, where γ^α are Dirac gamma matrices. Using magnetic moment of neutron we can calculate its contribution to the EDM generated by ALP exchange at 1-loop level (see, e. g., Eq. (5) and Fig. 4 for detail), the regarding $g_2(y)$ structure of the Feynman integral can be written as

$$g_2(y) = k_n \int_0^1 dx \frac{(1-x)(1-x^2)}{(1-x)^2 + y^2 x}, \quad (8)$$

where $y = m_a/m_N$. Analytic expression for the loop integrals $g_i(y)$ is presented in Appendix A.

The boundaries for combination of couplings $|g_s^\psi g_p^\psi|$ [56, 74] as a function of the ALP mass m_a are shown in Fig. 3. Difference of behavior different boundaries is connected with mass of fermions and existed limits to EDM of ones ($|d_e| < 1.1 \cdot 10^{-29} \text{ e} \cdot \text{cm}$, $|d_\mu| < 1.8 \cdot 10^{-19} \text{ e} \cdot \text{cm}$ and $|d_n| < 1.8 \cdot 10^{-26} \text{ e} \cdot \text{cm}$ see PDG Ref. [78]). Bounds on $|g_s^n g_p^n|$ from neutron EDM for light mass of ALPs are proportional to $\bar{\theta}$, parameter of CP -violation of vacuum in the quantum chromodynamics (QCD) which typical value is $\sim 10^{-10}$ [79, 80]. It is general for neutron EDM feature due the light scalar/pseudoscalar boson exchange in one loop [80] or two loops with CP -violation vertex [79, 81–83].

However from EDM of fermions we can estimate only the combination of ALPs couplings g_s^ψ and g_p^ψ . Wherein we want to note that the Lagrangian with universal CP -violating couplings to the SM fermions

$$\mathcal{L}_{QP} \supset \sum_\psi \bar{\psi} a (g_\psi^s + i g_\psi^p \gamma_5) \psi, \quad (9)$$

plays important role in spin interaction. In particular, by exploiting the data on Schiff moments of atoms or molecules its is straightforward to constrain the combination of couplings $|g_N^s g_e^p|$ (see, e. g., Refs. [74, 77, 84] for detail).

We would like to stress that the ALPs in the considered scenario could contribute to the fermion EDMs. Corresponding matrix element is induced by the CP -violating

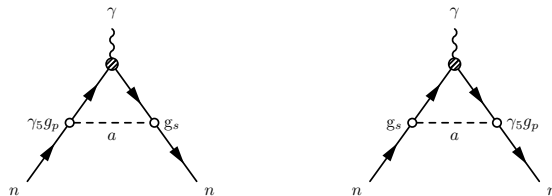


FIG. 2. Feynman diagrams with taking into account ALPs which generate neutron EDM induced by nonminimal electromagnetic couplings (anomalous magnetic moments) with external electromagnetic field (shaded blob).

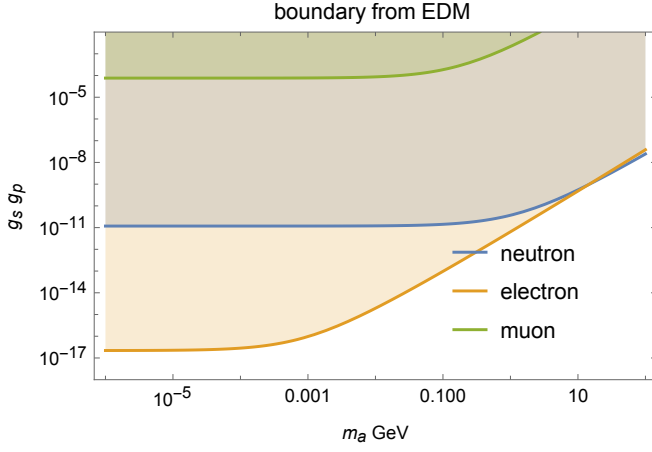


FIG. 3. Boundaries for the product of scalar and pseudoscalar couplings from EDM neutron and electron/muon as the function of the ALP mass. These boundaries correspond to leptophilic and hadrophilic scenarios.

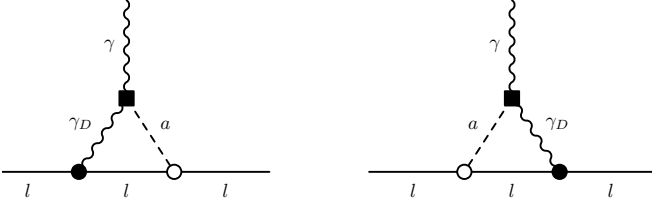


FIG. 4. Feynman diagrams which generate EDM terms due to axion with both dark and SM photons (see, e. g., Eq. (10) for detail).

diagrams analogous to the Barr-Zee diagrams with ALPs exchange in loop (see Fig.4). This contribution is generated by an additional interaction Lagrangian containing three terms: (i) P -parity violating coupling of ALP with SM fermions, (ii) P -parity conserving coupling of ALP with SM photon and dark photon, and (iii) P -parity conserving coupling of dark photon with SM fermions,

$$\mathcal{L} \supset a \left[g_s \bar{\psi} \psi + \frac{g_a \gamma_D}{2} F_{\mu\nu} \tilde{F}'^{\mu\nu} \right] + e \epsilon \bar{\psi} \gamma^\mu A'_\mu \psi. \quad (10)$$

The detailed analysis of present bounds would require the consideration of both the vector portal and dark ALP portal scenarios. Such analysis is beyond the scope of the present paper and we leave it for future study. In particular, we consider regarding limits elsewhere [85], just collecting some general formulas in Appendix B.

IV. THE MISSING ENERGY SIGNAL

In this section we discuss the setups for the fixed target experiments such as NA64e [31–35], LDMX [61–66], NA64μ [57–60] and M³ [67, 68], which can potentially

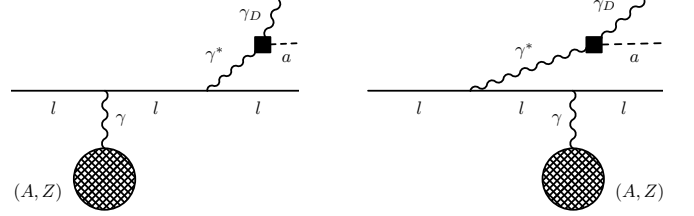


FIG. 5. Feynman diagrams for the radiate ALP and dark photon production by an impinging lepton on a nucleus Z . The regarding process represents the missing energy signature for the minimal dark ALP portal scenario $\mathcal{L} \supset \frac{1}{2} g_a \gamma_D a F_{\mu\nu} \tilde{F}'^{\mu\nu}$. Note that we neglect in the calculation the diagrams with off-shell photon from the nucleus leg, since its contribution to the signal process is suppressed by a factor of $(Z m_l / M_Z)^2$ for both electron and muon impinging on the nucleus.

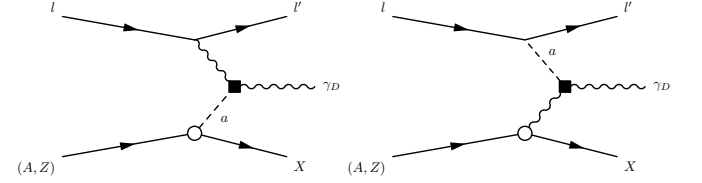


FIG. 6. Feynman diagrams for processes of the lepton scattering off atomic target (A, Z) in which the SM and dark photon interact through the axion portal coupling for both ALP-hadrophilic (left) and ALP-leptophilic (right) scenarios.

probe the invisible signatures associated with a lepton missing energy process

$$lZ \rightarrow Zl(E_{\text{miss}}), \quad (11)$$

where $l = (e, \mu)$ is the label either for electron or muon beam and Z designates the target nucleus. For instance, in the framework of the minimal dark ALP portal scenario the missing energy of the lepton beam E_{miss} can arise from the production of ALP a and dark photon γ_D by the off-shell photon γ^* in the process $lZ \rightarrow lZ\gamma^* \rightarrow lZa\gamma_D (\rightarrow \bar{\chi}\chi)$ (see, e. g., Fig. 5 for detail). To calculate the regarding yield we use state-of-the-art CalcHEP package [86].

In addition, for the hadron-specific and lepton-specific couplings of the ALPs the missing energy process $lZ \rightarrow lZ\gamma_D (\rightarrow \bar{\chi}\chi)$ is possible. This reaction implies that dark photon production is associated with interaction of ALP with SM photon which is produced either by beam or target (see, e. g., Fig. 6 for detail). To calculate cross-section of these processes we exploit the approximation of equivalent photon, also known as the Weizsacker-Williams (WW) [87–89] approximation. This approach is common for DM production study in the beam dump

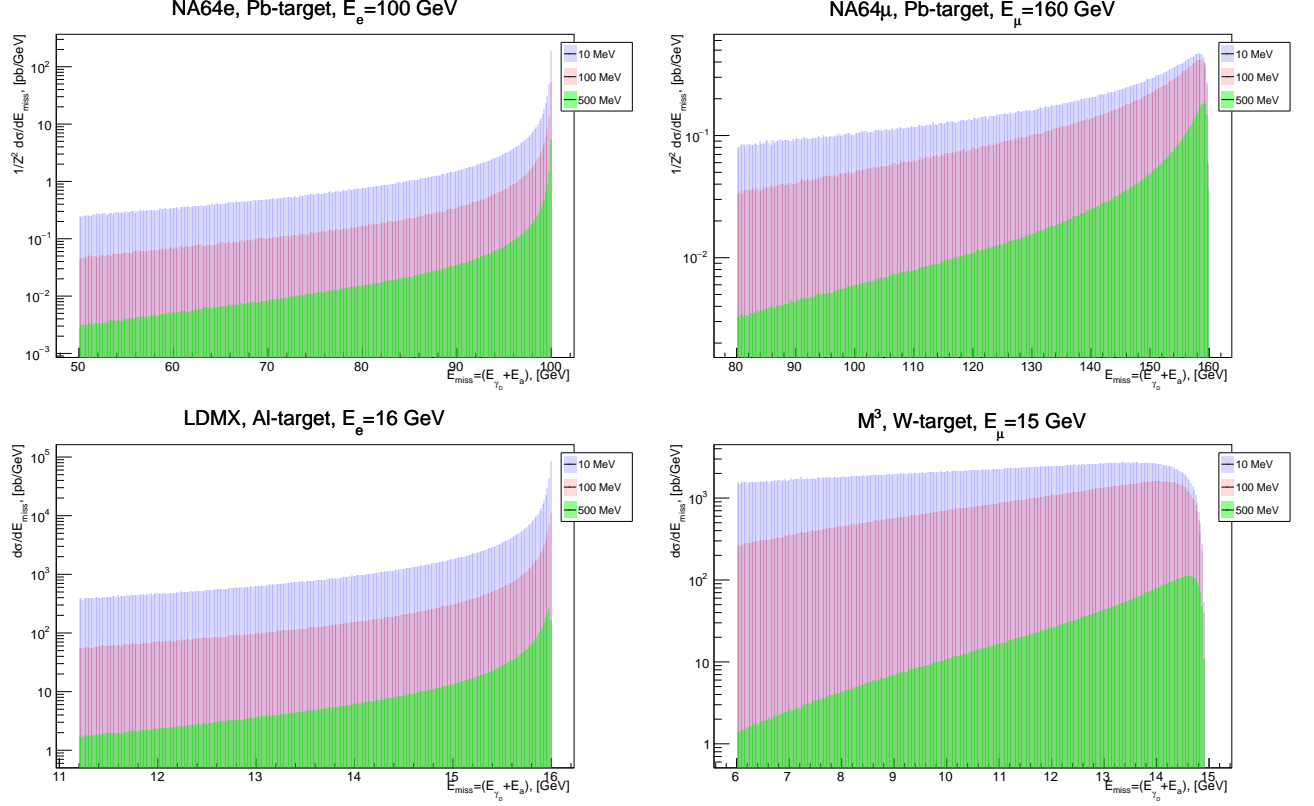


FIG. 7. The differential spectra of the process $lZ \rightarrow lZa\gamma_D (\rightarrow \chi\bar{\chi})$ as function of the missing energy $E_{miss} = E_{\gamma_D} + E_a$ for various experimental fixed target facilities and for the set of dark photon masses, $m_{\gamma_D} = 10$ MeV, $m_{\gamma_D} = 100$ MeV and $m_{\gamma_D} = 500$ MeV in the framework of minimal dark ALP portal scenario. We set $g_{a\gamma\gamma_D} = 1 \text{ GeV}^{-1}$ and $m_a = 10 \text{ keV}$.

and fixed target experiments. It implies replacing the fast moving charged particles by a specific photon distribution.

The dark photon can decay through the different channels in the dark ALP portal scenario. In particular, as soon as $m_{\gamma_D} \gtrsim m_a$ the visible two-body decay through the ALP and photon is kinetically accessible with a decay width [49]

$$\Gamma_{\gamma_D \rightarrow a\gamma} = \frac{g_{a\gamma\gamma_D}^2}{96\pi} m_{\gamma_D}^3 \left(1 - \frac{m_a^2}{m_{\gamma_D}^2}\right)^3. \quad (12)$$

Lagrangian (3) implies that the invisible two-body decay of dark photon γ_D into $\bar{\chi}\chi$ pair is also allowed with a decay width [90]

$$\Gamma_{\gamma_D \rightarrow \bar{\chi}\chi} = \frac{g_D^2}{12\pi} m_{\gamma_D} \left(1 + \frac{2m_\chi^2}{m_{\gamma_D}^2}\right) \left(1 - \frac{4m_\chi^2}{m_{\gamma_D}^2}\right)^{1/2}. \quad (13)$$

In the present paper we will focus on the process of invisible channel of dark photon decay into pair of hidden dark fermions, $\gamma_D \rightarrow \bar{\chi}\chi$ with $\text{Br}(\gamma_D \rightarrow \bar{\chi}\chi) \simeq 1$ for $m_\chi \ll m_{\gamma_D}$. That implies the following condition on decay widths $\Gamma_{\gamma_D \rightarrow \bar{\chi}\chi} \gg \Gamma_{\gamma_D \rightarrow a\gamma}$ and as a result this

yields $g_D \gg g_{a\gamma\gamma_D} m_{\gamma_D}$. Therefore it leads to the rapid decay of dark photon into $\bar{\chi}\chi$ pair after its production. In addition, in our analysis throughout the paper we keep the ALP mass m_a well below m_{γ_D} , such that $m_a \ll m_{\gamma_D}$, to get rid of the possible visible decay signatures $a \rightarrow \gamma\gamma_D$ in the detector of the fixed target facility.

To begin with, we estimate the number of missing energy events for the lepton beam at fixed target as follows

$$N_{sign} \simeq \text{LOT} \cdot \frac{\rho N_A}{A} L_T \int_{x_{min}}^{x_{max}} dx \frac{d\sigma(E_l)}{dx} \text{Br}(\gamma_D \rightarrow \chi\bar{\chi}), \quad (14)$$

where E_l is the initial energy of the beam, A is atomic weight number of target material, N_A is Avogadro's number, LOT is number of leptons accumulated on target, ρ is target density, L_T is the effective thickness of the target, $d\sigma/dx$ is differential cross-section for the specific missing energy channel $lZ \rightarrow lZl(E_{miss})$, x_{min} and x_{max} are the minimal and maximal fraction of the lepton energy $x = E_{miss}/E_l$ that hidden particles carry away. The cuts on x are determined by specific fixed-target facility.

Let us discuss now the benchmark input parameters for the specific experimental setup.

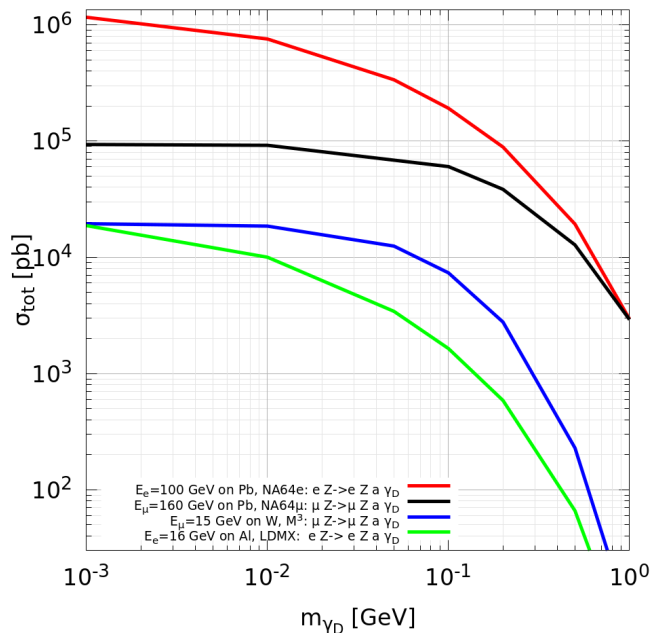


FIG. 8. The total cross-section as a function of the mass m_{γ_D} for the minimal portal scenario, $m_a \simeq 10$ keV. We set here $g_{a\gamma_D} = 1 \text{ GeV}^{-1}$ and integrate the cross-section over the experimental cut range $x_{\min} \lesssim x \lesssim x_{\max}$. Red line is the cross-section for the NA64e experiment, black line corresponds to NA64mu experiment, blue line is the total cross-section for M³ experiment and green line corresponds to the cross-section of the LDMX facility.

A. The NA64e experiment

The dark photon and/or ALP can be produced in the reaction of high-energy electrons of $E_e = 100$ GeV scattering off nuclei of an active lead ECAL target

$$eZ \rightarrow eZ\gamma_D(a), \quad (15)$$

followed by prompt $\gamma_D \rightarrow \bar{\chi}\chi$ decay into dark matter particles (χ). Thus, the fraction $E_{\text{miss}} = xE_e$ of the primary beam energy is carried away by the χ 's (a) which penetrate the detector of NA64e without energy deposition. The remaining part of the beam energy fraction $E_e^{\text{rec}} \equiv E_e(1-x)$ is deposited in the ECAL target by the scattered electrons. Therefore, the occurrence of the hidden particles produced in the process (11) leads to an excess of events with a single electromagnetic (EM) shower with energy E_e^{rec} above the expected background (see, e. g., Ref. [30] for detail). In the present analysis, we conservatively assume that the EM shower is localized in the first radiation length of the lead detector $X_0 = 0.56$ cm, such that the effective thickness of the target in (14) is $L_T \simeq X_0$. That implies that the dominant production of the hidden particles occurs within first radiation length of the active ECAL target [91]. The candidate events are requested to have the missing energy in the range $E_e^{\text{rec}} \lesssim 0.5E_e$, implying that $x_{\min} = 0.5$ in Eq. (14).

The ECAL target of NA64e is a matrix of 6×6 Shashlyk-type modules assembled from lead (Pb) ($\rho = 11.34 \text{ g cm}^{-3}$, $A = 207 \text{ g mole}^{-1}$, $Z = 82$) and scintillator (Sc) plates. Note that production of hidden particles in the scintillator is subleading due to its larger radiation length, $X_0(\text{Sc}) \gg X_0(\text{Pb})$, thus we ignore it in the calculation.

The NA64e employs the optimized electron beam from the H4 beam line at the SPS. The maximum intensity of the beam is $\simeq 10^7$ electrons per spill of 4.8 s, the number of good spills per day is estimated to be 4000. Therefore, approximately 120 days are required to accumulate 5×10^{12} electrons on target (EOT) at the H4 electron beam line.

B. The LDMX experiments

The LDMX is the proposed fixed target experiment at Fermilab that exploits the electron beam as well as the NA64e facility. The LDMX is designed to measure missing momentum of the electron, thus probing of the process (15) at LDMX is complementary to NA64e. Moreover, the missing momentum cuts and the active veto systems of both experiments make them essentially background free Ref. [30, 62]. The proposed LDMX facility consists of a target, silicon tracker system, electromagnetic and hadron calorimeter (for details, see, e. g., Refs. [62, 66]). The most of the electron beam energy is lost due to the emission of the dark particles occurring in the thin upstream target. The missing momentum of the electron is tagged by the silicon tracker, downstream electromagnetic and hadron calorimeter. The final state electron missing energy cut is chosen to be $E_e^{\text{rec}} \lesssim 0.3E_e$, that corresponds to $x_{\min} = 0.7$ in Eq. (14). In our analysis we carry out the calculation for the aluminium-target (Al) ($X_0 = 8.9$ cm, $\rho = 2.7 \text{ g cm}^{-3}$, $A = 27 \text{ g mole}^{-1}$, $Z = 13$) with a thickness of $L_T \simeq 0.4X_0$. Note that the LDMX plans to accumulate EOT $\simeq 10^{16}$ with the beam energy up to $E_e = 16$ GeV for the final phase of running after 2027 [66].

C. The NA64mu experiment

The NA64mu facility [59, 60] is a complementary experiment to the NA64e that searches for the dark sector particles in the muon beam mode

$$\mu Z \rightarrow \mu Z\gamma_D(a). \quad (16)$$

In our calculations we set the muon beam energy of NA64mu to be $E_\mu \simeq 160$ GeV, the muon flux is chosen to be about MOT $\simeq 5 \times 10^{13}$ for the projected statistics. We consider the lead shashlyk-type electromagnetic calorimeter that serves a target with a typical thickness of $L_T \simeq 40X_0 \simeq 22.5$ cm. We also neglect the muon stopping loss in the lead target [92, 93], since its

typical energy attenuation is rather small $\langle dE_\mu/dx \rangle \simeq 12.7 \times 10^{-3} \text{ GeV/cm}$ for the ultra-relativistic approach $E_\mu \simeq 160 \text{ GeV}$.

The NA64 μ facility exploits to magnet spectrometers allowing for precise measurements of momenta for incident and outgoing muons [60]. We set the following cut on the energy of recoiling muon $E_\mu^{rec} \lesssim 0.5E_\mu \simeq 80 \text{ GeV}$, so that $x_{min} = 0.5$.

We also note that the intensity of 160 GeV muons at the M2 beam line can be a higher by factor of 10 than that for the electrons. Therefore, about the same running time of 120 days is required to accumulate a much higher statistics of 5×10^{13} muons on target (MOT) relative to EOT = 5×10^{12} for NA64e.

D. The M³ experiments

The M³ (muon missing momentum) experiments at Fermilab [67] is the projected modification of LDMX facility that is suitable for probing the muon-specific missing energy signatures, $\mu Z \rightarrow \mu Z \gamma_D(a)$. In particular, it considers new physics discovery potential for the muon beam of $E_\mu \simeq 15 \text{ GeV}$, thick tungsten target (W) ($X_0 \simeq 0.35 \text{ cm}$, $\rho = 19.3 \text{ g cm}^{-3}$, $A \simeq 184 \text{ g mole}^{-1}$, $Z = 74$) of thickness of $L_T = 50X_0 \simeq 17.5 \text{ cm}$ and downstream detector to veto SM backgrounds.

The M³ plans to accumulate 10^3 MOT within $\simeq 3$ months of data taking. The signal missing momentum signature of the recoil muon is $E_\mu^{rec} \lesssim 9 \text{ GeV}$, meaning that $x_{min} = 0.4$ in Eq. (14). The reported [67] muon stopping loss is 530 MeV through a tungsten target of $50X_0$ for muons of $E_\mu \simeq 15 \text{ GeV}$. So that we neglect $\langle dE/dx \rangle$ in the signal estimate for the sake of simplicity. Given that approach one can exploit the Eq. (14) for the signal yield estimate.

V. MINIMAL DARK ALP PORTAL SCENARIO

In this section for the minimal dark ALP portal setup (3) we discuss the experimental signature of dark photon and ALP production in the processes

- $e(\mu)Z \rightarrow e(\mu)Z\gamma^* \rightarrow e(\mu)Za\gamma_D$ that is shown in Fig. 5 for the fixed target experiments,
- J/ψ vector meson photoproduction, $eZ \rightarrow eZJ/\psi$ followed by invisible decay $J/\psi \rightarrow a\gamma_D$, at NA64e experiment (see e. g. Fig. 10 for details),
- $e^+e^- \rightarrow \gamma\gamma^* \rightarrow \gamma(\gamma^* \rightarrow a\gamma_D) \rightarrow \gamma a\gamma_D$ that is shown in Fig. 11 for BaBar experiment.

In particular, we estimate the rate of these processes and calculate the sensitivity curves from the null result of the experimental facilities.

A. Radiative cross-sections of the fixed target facilities

In order to estimate the sensitivity of the lepton fixed target experiments to probe minimal dark ALP portal missing energy signatures we calculate cross-sections by exploiting state-of-art **CalcHEP** package [86]. In the SM model of **CalcHEP** we added both the massive ALP a and dark photon γ_D as the new particles by including the corresponding interaction Lagrangian with photon $\mathcal{L} \supset (1/2)g_{a\gamma\gamma_D}aF_{\mu\nu}\tilde{F}'_{\mu\nu}$. We also added the target nucleus with atomic number A , charge Z with spin $1/2$ particle and with mass M_Z that couples the SM photon via $U(1)$ vertex $ieZF(t)\gamma_\mu$, where $t = -q^2 > 0$ is a nucleus transfer momentum squared, $F(t)$ is an elastic form-factor, that can be written as follows

$$F(t) = \frac{a^2 t}{(1 + a^2 t)} \frac{1}{(1 + t/d)}, \quad (17)$$

here $a = 111Z^{-1/3}/m_e$ and $d = 0.164A^{-2/3} \text{ GeV}^2$ are the form-factors parameters of screening and nucleus size respectively [94, 95]. Form factor specified in Eq. (17) was implemented in the **C++** files for the expression of the matrix element squared, $|\mathcal{M}(lZ \rightarrow lZa\gamma_D)|^2$, that is generated in the analytical session of the **CalcHEP**.

Given the input parameters of the experiments discussed in Sec. IV we carry out the integration of the exact tree-level amplitude squared $e(\mu)Z \rightarrow e(\mu)Za\gamma_D$ over the phase space of the outgoing particles by exploiting the **CalcHEP** package. In particular, for the specific chemical element of the target and typical energies of the lepton beam E_l , we calculate σ_{tot} as a function of the mass m_{γ_D} in the range $1 \text{ MeV} \lesssim m_{\gamma_D} \lesssim 1 \text{ GeV}$ for $m_a \simeq 10 \text{ keV}$. The numerical integration was performed by the **VEGAS** importance sampling algorithm with $N_{session} = 10$ runs and $N_{calls} = 10^6$ sampling points during each run. The grid adapting of the **VEGAS** algorithm was performed with a fairly good accuracy of $\mathcal{O}(0.1)\% - \mathcal{O}(0.01)\%$ in the numerical session of **CalcHEP**.

In Fig. 7 we show the differential cross-sections as a function of the missing energy, $E_{miss} = E_{\gamma_D} + E_a$, in the signal box range $E_l^{th} \lesssim E_{miss} \lesssim E_l$ for the fixed target experiments and various masses m_{γ_D} , here we denote $E_l^{th} = x_{min}E_l$. Both the NA64e and LDMX cross-sections have a peak at $E_{miss} \simeq E_e$. Which implies that the signal is strongly forward peak for $E_{miss} \gg m_{\gamma_D}, m_a$ and the dominant part of the beam energy transfers to the $a\gamma_D$ pair. However for both muon beam cross-sections of NA64 μ and M³ the peak at $E_{miss} \lesssim E_\mu$ is mitigated since the production rates of $a\gamma_D$ pair are in the soft bremsstrahlung-like regime as long as $m_{\gamma_D}, m_a \lesssim m_\mu$.

In Fig. 8 the resulted total cross-sections are shown for NA64e, NA64 μ , LDMX and M³ experimental facilities. It is worth mentioning that the NA64e cross-section σ_e^{tot} in Fig. 8 for the lead (Pb) target ($Z \simeq 82$) with impinging electron beam of $E_e = 100 \text{ GeV}$ is generally larger by a

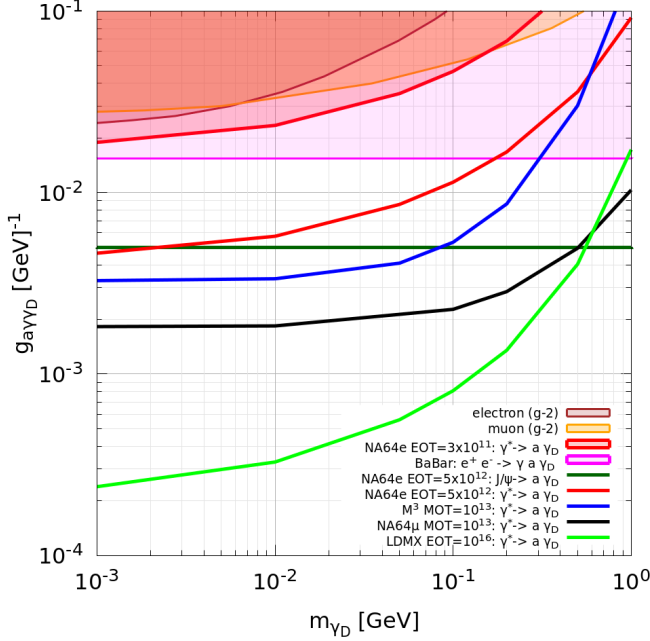


FIG. 9. The limits on $g_{a\gamma\gamma_D}$ coupling from the fixed-target experiments and BaBar for the minimal dark ALP portal setup as a function of the dark photon mass m_{γ_D} . For all sensitivity curves we imply that $\text{Br}(\gamma_D \rightarrow \chi\bar{\chi}) \simeq 1$ and $m_a = 10 \text{ keV}$. Red line is the projected sensitivity for NA64e experiment, black line corresponds to NA64 μ facility, blue line is the expected reach of M^3 , and green line corresponds to the projected sensitivity of LDMX facility. The shaded red region shows the parameter space excluded by the NA64e experiment for $\text{EOT} \simeq 3 \times 10^{11}$. At 90% CL the excluded region of NA64e experiment rules out the possible explanation of $(g-2)$ muon (shaded orange region) and electron (shaded brown region) anomalies [3, 96, 97] by the minimal ALP scenario at 2-loop level [48]. The BaBar pink shaded region refers to search for the three body monophoton process $e^+e^- \rightarrow a\gamma\gamma_D$ followed by the rapid decay into DM pair $\gamma_D \rightarrow \chi\bar{\chi}$. Dark green line represents the expected reach of NA64e experiment associated with J/ψ meson photoproduction followed by invisible decay $J/\psi \rightarrow a\gamma_D$ for $\text{EOT} \simeq 5 \times 10^{12}$.

factor of $\simeq 10$ than the lead cross-section $\sigma_{\mu}^{\text{tot}}$ for the muon beam of $E_{\mu} = 160 \text{ GeV}$. Therefore, there is a cross-section advantage of using the electron beam instead of muon beam in the low mass region $m_{\gamma_D} \gtrsim 1 \text{ MeV}$ as long as both electron and muon have the typical energies of the order of $E_{\mu} \simeq E_e \simeq \mathcal{O}(100) \text{ GeV}$. On the other hand, σ_e^{tot} decreases more rapidly than $\sigma_{\mu}^{\text{tot}}$ as m_{γ_D} increases towards 1 GeV in the mass range of the interest $m_{\gamma_D} \lesssim 1 \text{ GeV}$. The latter one scales as $\sigma_{\mu}^{\text{tot}} \propto g_{a\gamma\gamma_D}^2$ and depends weakly on m_{γ_D} for the bremsstrahlung-like regime as long as $m_a, m_{\gamma_D} \ll m_{\mu}$.

In addition, one can see from Fig. 8 that LDMX cross-section for the aluminium (Al) target ($Z \simeq 13$) is smaller than cross-section for the lead target of NA64e facility, since the rate of $a\gamma_D$ production scales with $\propto Z^2$ and the aluminium nucleus charge is smaller by factor of $82/13 \simeq$

6.3.

However, if we compare the M^3 cross-section for the tungsten (W) target ($Z \simeq 74$) with impinging muon beam of $E_{\mu} \simeq 15 \text{ GeV}$ and LDMX cross-section with impinging electrons of $E_e \simeq 16 \text{ GeV}$, one can conclude that the advantage of the electron beam exploiting in the low mass region $m_{\gamma_D} \gtrsim 1 \text{ MeV}$ is compensated by the nucleus charge suppression. As the result, both cross-sections of the M^3 and LDMX are of the same order of the magnitude at $m_{\gamma_D} \simeq 1 \text{ MeV}$.

B. Limits from the fixed target experiments

Using the formula (14) for the number of produced $a\gamma_D$ pairs and the results on the production cross-sections, we find the expected bounds on the coupling $g_{a\gamma\gamma_D}$ for the minimal dark ALP portal scenario. We require $N_{\text{sign}} \gtrsim 2.3$ that corresponds to the 90% CL exclusion limit on coupling $g_{a\gamma\gamma_D}$ for the background free case and null-result of the fixed target experiments. In Fig. 9 we show the expected reach of NA64e, LDMX, NA64 μ and M^3 . Note that projected limits on $g_{a\gamma\gamma_D}$ from LDMX are fairly strong, even though the cross-section of $a\gamma_D$ pair production at LDMX is relatively small (see, e. g., green line in Fig. 8). The regarding LDMX sensitivity enchantment can be explained by the large number of the projected accumulated statistics, $\text{EOT} \simeq 10^{16}$, by the final phase of experimental running. In addition, we note also from the M^3 and NA64 μ cross-section shown in Fig. 8 that the signal of $a\gamma_D$ pair production by muon beam drops as the energy of muons decreases. In particular, compared to M^3 option with 16 GeV beam muons, a higher energy, e. g. 160 GeV , muons of NA64 μ allows for probing wider region in the parameter space of the minimal dark ALP portal scenario for $\text{MOT} = 10^{13}$. In addition, we note that the projected limits of NA64e for $\text{EOT} \simeq 5 \times 10^{12}$ can be ruled out by other fixed target experiments.

In Fig. 9 we show by the shaded red region the excluded limits of NA64e for the current accumulated statistics [34] of $\text{EOT} \simeq 3 \times 10^{11}$. This region rules out at 90% CL the typical parameter space of minimal dark ALP portal scenario [48] that can explain the $(g-2)_{\mu}$ and $(g-2)_e$ anomalies [3, 96–98] at two loop level. That contribution of ALP and dark photon is analogous to neutral pion term [99] that contributes the 2-loop hadronic part of charged fermion $(g-2)_f$.

Concluding this subsection we note that there is detector advantage of exploiting the muons at NA64 μ instead of electrons at NA64e, even though both experiments have a target of total equivalent thickness of $40X_0 \simeq 22.5 \text{ cm}$. The key point of that idea is the following [93]. The electron beam of $E_e \simeq 100 \text{ GeV}$ degrades significantly within first radiation length X_0 of the lead target. Contrary, the muons pass the target without significant loss of the energy, since their radiation length scales as $X_0^{\mu} \simeq (m_{\mu}/m_e)^2 X_0 \gg X_0$. This

implies that missing momentum signal of NA64 μ is scaled as $N_{sign} \propto L_T$. So that, one can improve the sensitivity of the muon beam mode by increasing the typical interaction length of the dump.

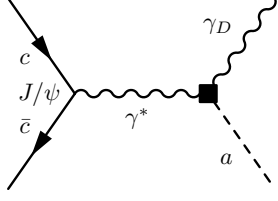


FIG. 10. Feynman diagrams for the radiative $J/\psi \rightarrow \gamma^* \rightarrow a\gamma_D$ decay.

C. Expected constraints from $J/\psi(1S) \rightarrow a\gamma_D$ decay at NA64e

In this subsection we follow Ref. [65, 100] to constrain the parameter space of the minimal ALP-portal scenario from invisible decay of $J/\psi \rightarrow a\gamma_D$ at NA64e. The matrix element of the charm quark and anti-quark transition process $c(p_1)\bar{c}(p_2) \rightarrow \gamma^*(q) \rightarrow a(k_2)\gamma_D(k_1)$ can be written as follows (see e. g. Fig. 10 for detail)

$$\mathcal{M}_{c\bar{c}} = ieQ_c\bar{v}(p_2)\gamma^\mu u(p_1)\frac{g_{\mu\nu}}{q^2}g_{a\gamma\gamma_D}\epsilon^{\nu\lambda\rho\sigma}k_\lambda^1q_\rho^2\epsilon_\sigma(k^1), \quad (18)$$

where k_1, k_2 and p_1, p_2 are, respectively, the four momenta of the ALP, dark photon and of the charm quarks. In the center of mass frame one has, $p_1 = p_2 = p = (m_c, 0, 0, 0)$ with m_c being the mass of the charm quark, while q in Eq. (18) is the photon four-momentum, such that $q^2 = 4m_c^2$, $Q_c = 2/3$ is the charge of the charm quark. By integrating the averaged amplitude squared $|\mathcal{M}_{cc}|^2$ (see e. g. Eq. (18)) over the phase space of outgoing particles one can obtain the invisible decay width

$$\Gamma_{J/\psi \rightarrow a\gamma_D} = \frac{|\psi_{J/\psi}(0)|^2}{8\pi}g_{a\gamma\gamma_D}^2e^2Q_c^2\left(1 - \frac{m_{\gamma_D}^2}{M_{J/\psi}^2}\right)^3, \quad (19)$$

where $M_{J/\psi} \simeq 3.1\text{ GeV}$ is the mass of J/ψ and $|\psi_{J/\psi}(0)|^2 \simeq 4.47 \times 10^{-2}\text{ GeV}^3$ is the squared radial wave-function [98] of J/ψ at the origin $r = 0$. In order to calculate $|\mathcal{M}_{cc}|^2$ we exploit the state-of-the-art **FeynCalc** package [101] of **Wolfram Mathematica** [102]. In Eq. (19) we neglect the ALP mass, $m_{\gamma_D} \gg m_a$. The authors provide in Tab. II of Ref. [65] the number of expected J/ψ vector mesons $N_{J/\psi} \simeq 1.1 \times 10^5$ produced for projected statistics $\text{EOT} \simeq 5 \times 10^{12}$ at NA64e. Therefore one can easily estimate the expected reach on $\text{Br}(J/\psi \rightarrow a\gamma_D) \lesssim 2.3/N_{J/\psi}$ at 90%CL that implies no

signal events of J/ψ invisible decays into $a\gamma_D$ pair at NA64e for the background free case. Here we use the value for the total decay width $\Gamma_{J/\psi}^{\text{tot}} \simeq 92.9\text{ keV}$ from Ref. [98]. That yields the expected reach on the coupling $g_{a\gamma\gamma_D} \lesssim 5 \times 10^{-3}\text{ GeV}^{-1}$ at 90%CL for NA64e in the mass range of interest $1\text{ MeV} \lesssim m_{\gamma_D} \lesssim 1\text{ GeV}$. In Fig. 9 we show the regarding expected limit that can rule out the limit of NA64e for $a\gamma_D$ -pair production in the process $eZ \rightarrow eZ\gamma^*(\rightarrow a\gamma_D)$ for the same statistics $\text{EOT} \simeq 5 \times 10^{12}$. Note that in the present analysis we conservatively assume that dominant channel of missing energy events at NA64e is associated with photoproduction of J/ψ meson $\gamma Z \rightarrow ZJ/\psi$ followed by its rapid decay $J/\psi \rightarrow a\gamma_D$ in the detector of NA64e. The production of ρ, ω and ϕ vector mesons at NA64e is expected to be subdominant [65, 103].

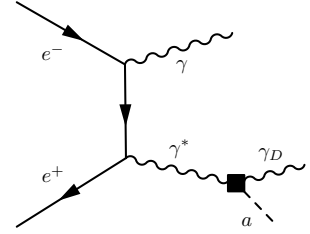


FIG. 11. Feynman diagrams for the monophoton three body process $e^+e^- \rightarrow a\gamma\gamma_D$ followed by invisible dark photon decay into DM fermion pair, $\gamma_D \rightarrow \chi\bar{\chi}$. That reaction is relevant for the BaBar constraints on $g_{a\gamma\gamma_D}$ coupling in the framework of the minimal dark ALP portal scenario.

D. Bounds from monophoton BaBar data

An authors of Ref. [48] provide an explicit analysis of the the mono-photon signal for the process $e^+e^- \rightarrow a\gamma_D$ followed by decay $\gamma_D \rightarrow a\gamma$ from BaBar data. They also provide the regarding exclusion limits (see e. g. Fig. 4 from Ref. [48]) in $(m_{\gamma_D}, g_{a\gamma\gamma_D})$ plane from BaBar experiment. These limits are not relevant for our minimal benchmark scenario, since we suppose that γ_D decays rapidly into $\chi\bar{\chi}$ pair with $\text{Br}(\gamma_D \rightarrow \chi\bar{\chi}) \simeq 1$ and thus visible monophoton decays $\gamma_D \rightarrow a\gamma$ are suppressed, $\text{Br}(\gamma_D \rightarrow a\gamma) \ll 1$. However, three body final state process $e^+e^- \rightarrow a\gamma\gamma_D$ is kinematically allowed for our analysis. That reaction is sub-leading relative to two-body final state process $e^+e^- \rightarrow a\gamma_D$. The regarding suppression can be found in Fig. 3 of Ref. [48] which shows the total cross-sections of the relevant processes as the function of mass m_{γ_D} . In particular, for the mass range $1\text{ MeV} \lesssim m_{\gamma_D} \lesssim 1\text{ GeV}$ and $g_{a\gamma\gamma_D} = 1\text{ GeV}^{-1}$ one has $\sigma_{\text{tot}}(e^+e^- \rightarrow a\gamma_D) \simeq 1.2 \times 10^5\text{ pb}$ and $\sigma_{\text{tot}}(e^+e^- \rightarrow a\gamma\gamma_D) \simeq 6 \times 10^3\text{ pb}$ for two body and three body final state respectively. Therefore it is straightforward to obtain the relevant for our analysis limit on $g_{a\gamma\gamma_D}^{(3\text{-body})}$ from

mono-photon bound $g_{a\gamma\gamma_D}^{(2-body)} \simeq 2 \times 10^{-3} \text{ GeV}^{-1}$ shown in Fig. 4 of Ref. [48]. Namely for the mass range of interest $1 \text{ MeV} \lesssim m_{\gamma_D} \lesssim 1 \text{ GeV}$ this yields:

$$g_{a\gamma\gamma_D}^{(3-body)} \simeq g_{a\gamma\gamma_D}^{(2-body)} \times \left(\frac{\sigma_{tot}(e^+e^- \rightarrow a\gamma_D)}{\sigma_{tot}(e^+e^- \rightarrow a\gamma_D)} \right)^{1/2} \simeq 1.5 \times 10^{-2} \text{ GeV}^{-1}. \quad (20)$$

As expected [48, 49], the experimental reach of the BaBar weakens by factor of approximately $\sqrt{20} \simeq 4.5$ for the $\text{Br}(\gamma_D \rightarrow \chi\bar{\chi}) \simeq 1$. In Fig. 9 we show the current constraint from BaBar monophoton signal $e^+e^- \rightarrow a\gamma\gamma_D$ by the shaded pink region. It rules out the current experimental constraints of the NA64e experiment for $\text{EOT} \simeq 3 \times 10^{11}$.

VI. NON-MINIMAL ALP-HADROPHILIC SCENARIO

In this section we calculate the cross-section dark photon production in the process $lZ \rightarrow lZ\gamma_D$ that is shown in left side of the Fig. 6 for the case of hadrophilic ALPs. That implies the benchmark coupling of the ALP and dark photons in the following form

$$\mathcal{L} \supset \mathcal{L}_{\text{dark axion portal}} + \bar{\chi}(\gamma^\mu i\partial_\mu - g_D \gamma^\mu A'_\mu + m_\chi)\chi + \sum_{N=n,p} a\bar{N}(g_\psi^s + ig_\psi^p \gamma_5)N. \quad (21)$$

For the sake of simplicity we consider benchmark universal scalar and pseudo-scalar coupling of ALP to nucleons, such that $g_p^s = g_n^s \equiv g^s$ and $g_p^p = g_n^p \equiv g^p$.

In order to calculate the cross-section of dark photon lepton-production at nucleus (A, Z) where A is nucleus mass number, Z is charge of nucleus, we use the equivalent photon approximation, that implies replacing the fast moving leptons by the photons following a distribution [104]

$$\gamma_l(x_\gamma, q_\perp^2) \simeq \frac{\alpha}{2\pi} \frac{1 + (1 - x_\gamma)^2}{x_\gamma} \frac{q_\perp^2}{(q_\perp^2 + x_\gamma^2 m_l^2)^2}, \quad (22)$$

where E_γ is the energy of the photon emitted by incoming lepton, x is fraction of the photon energy defined as $x_\gamma \equiv E_\gamma/E_l$, here E_l is energy of oncoming lepton, m_l is the lepton mass, q_\perp is the photon transfer momentum. Note that q_\perp^2 is typically very small, $q_\perp \ll E_l, E_\gamma$. The total cross section of dark photon lepton-production at nucleus can be written as

$$\sigma_{lZ \rightarrow lZ\gamma_D} = \int dx dq_\perp^2 \gamma_l(x_\gamma, q_\perp^2) \int dt \frac{d\sigma_{\gamma Z \rightarrow Z\gamma_D}}{dt}, \quad (23)$$

where the cross-section of dark photon production can be written as sum of partial cross-sections for each nucleon N in nuclear of target

$$\frac{d\sigma_{\gamma Z \rightarrow Z\gamma_D}}{dt} = A \frac{d\sigma_{\gamma N \rightarrow N\gamma_D}}{dt},$$

The Lorentz invariant form of differential cross section of dark photon production due to photon scattering on nucleon is

$$\frac{d\sigma_{\gamma N \rightarrow N\gamma_D}}{dt} = \frac{\frac{1}{4} \sum_{\text{pol}} |M_{\gamma N}|^2}{16\pi\lambda(s, m_N^2, 0)}, \quad (24)$$

where $\lambda(s, m_N^2, 0) = (s - m_N^2)^2 = 4m_N^2 E_\gamma^2$ is the Källén function in the rest frame of initial nucleon. Then the square of the magnitude of matrix element is given by

$$|M_{\gamma N}|^2 \simeq \frac{g_{a\gamma\gamma_D}^2}{2} \frac{(t - m_{\gamma_D}^2)^2}{(t - m_a^2)^2} m_N^2 \times \left[g_s^2 - g_p^2 + (g_s^2 + g_p^2) \frac{E_{2N}}{m_N} \right], \quad (25)$$

where $E_{2N} \simeq m_N - t/(2m_N)$ is the energy of the outgoing nucleon in the laboratory frame, t is the nucleon transfer momentum squared, such that $t \equiv -2m_N(E_\gamma - E_{\gamma_D})$, for the nearly collinear emission of dark photon this yields

$$t \simeq -E_\gamma^2 \theta_{\gamma_D}^2 - m_{\gamma_D}^4 / (4E_\gamma^2).$$

It is worth mentioning that for the small angles of dark photon production the amplitude squared Eq. (25) is suppressed if we put $g_N^s = 0$ and $g_N^p \neq 0$. The regarding suppression factor is associated with the term

$$|M_{\gamma N}|^2 \propto (g_N^p)^2 (E_{2N} - m_N)/m_N \ll 1$$

as long as $\theta_{\gamma_D} \ll 1$ and $E_{2N} \simeq m_N$. Otherwise, if we set $g_N^p = 0$ and $g_N^s \neq 0$ one gets

$$|M_{\gamma N}|^2 \propto (g_N^s)^2 E_{2N}/m_N.$$

As a result, the cross-section for the scalar-specific couplings of nucleons is enhanced by factor of approximately $\simeq E_{2N}/(E_{2N} - m_N)$ relative to the pseudo-scalar-specific cross-section. If one sets $g_p = g_s = g_N$ then for $t \ll m_a^2, m_{\gamma_D}^2$ we get the following expression for the amplitude squared

$$|M_{\gamma N}|^2 \simeq g_{a\gamma\gamma_D}^2 g_N^2 m_N^2 \left(\frac{m_{\gamma_D}}{m_a} \right)^4 \left[1 + \mathcal{O}\left(\frac{m_{\gamma_D}^2}{E_\gamma^2} \right) \right]. \quad (26)$$

The Eq. (26) implies that for the highly collinear emission of the dark photon (negligible momentum transfer) its production rate grows as $\propto (m_{\gamma_D}/m_a)^4$ for increasing m_{γ_D} . In fact, the nucleon momentum transfer can not be completely neglected and the realistic cross-section grows a bit more slowly than $(m_{\gamma_D}/m_a)^4$ as $m_{\gamma_D} \gtrsim \mathcal{O}(100) \text{ MeV}$.

Finally, one can obtain the double differential cross-section of dark photon production

$$\frac{d\sigma_{lZ \rightarrow lZ\gamma_D}}{dE_{\gamma_D} d\theta_{\gamma_D}} \simeq \frac{1}{E_l} \int dq_\perp^2 \gamma_l(E_{\gamma_D}/E_l, q_\perp^2) \frac{d\sigma_{\gamma Z}}{d\theta_{\gamma_D}}. \quad (27)$$

In Fig. 12 we show the differential cross-section $(d\sigma/d\theta_{\gamma_D})_{lZ \rightarrow lZ\gamma_D}$ as the function of θ_{γ_D} in the range

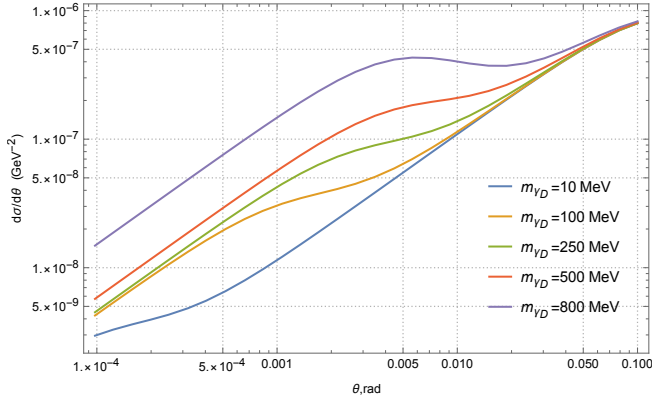


FIG. 12. The differential cross-section by angle of dark photon production at fixed target of NA64e in hadrophilic-ALP portal for various dark photon masses m_{γ_D} and for small values of angle θ between dark photon and photons from beam. We set parameters as $m_a = 10$ keV, $g^s = g^p = 1$, $g_{a\gamma\gamma_D} = 1$ GeV $^{-1}$, $E_e = 100$ GeV.

of small dark photon emission angle $\theta_{\gamma_D} \lesssim 0.1$. As we mentioned above, the larger masses m_{γ_D} imply the larger values of the differential cross-section. That dependence can be described also in terms of specific Lorentz invariant characteristics. Let us consider the characteristic function for the benchmark case [105]

$$g_{\gamma_D} = (s - m_N^2) / (s - m_{\gamma_D}^2 + m_N^2) \times \lambda^{\frac{1}{2}}(s, m_N^2, 0) / \lambda^{\frac{1}{2}}(s, m_{\gamma_D}^2, m_N^2), \quad (28)$$

that is associated with the typical angles of dark photon emission in the laboratory frame. It is straightforward to obtain that $g_{\gamma_D} > 1$ for $m_{\gamma_D} \lesssim 100$ MeV, which means that $\theta_{\gamma_D} \ll 1$, i.e. the cross-section peaks forward. On the other hands, one can obtain that $g_{\gamma_D} < 1$ as soon as $m_{\gamma_D} \gtrsim 1$ GeV, therefore the typical momentum of dark photon γ_D production can be not collinear to the beam line in this case, i. e. the typical angles θ_{γ_D} can be as large as $\theta_{\gamma_D} \gtrsim 1$. In the present paper we study the elastic production of dark photon, so that in the analysis for simplicity we conservatively set the typical maximum angle of dark photon emission to be $\theta_{\gamma_D} \lesssim \theta_{max} \equiv 0.1$. The total cross-section of the dark photon production is calculated for the regarding angle cut, which however decreases significantly the signal rate of γ_D emission.

However, for the ALP-hadrophilic scenario it is worth to calculate the inelastic photo-production cross-section of γ_D that implies large nucleon transfer momentum and relatively wide emission angle $\theta_{\gamma_D} \gtrsim 1$. That analysis would require the realistic simulation of the experimental efficiency and the hadronic response in the detector. This, however is beyond the scope of the present paper and we leave such analysis for future study.

In Fig. 14 of Sec. VIII the 90% C.L. sensitivity curves of the fixed target experiments are shown for the combination of couplings $|g_{a\gamma\gamma_D} g_N|$. In order to plot these curves we set $N_{sign} > 2.3$, implying Poisson statistics for

the signal events, background free case and null result for the DM detection.

VII. NON-MINIMAL ALP-LEPTOPHILIC SCENARIO

In this section we consider the process

$$l(p)Z(\mathcal{P}_i) \rightarrow l(p')Z(\mathcal{P}_f)\gamma_D(k), \quad (29)$$

shown in the right panel of Fig. 6 for the leptophilic ALP, where $p = (E_l, \mathbf{p})$ and $p' = (E'_l, \mathbf{p}')$ are the four momenta of initial and outgoing leptons, respectively, $\mathcal{P}_i = (M_N, \mathbf{0})$ and $\mathcal{P}_f = (\mathcal{P}_f^0, \mathbf{P}_f)$ are the four-momenta of initial and outgoing nuclei, respectively, here M_N is the mass of the nucleus and $k = (E_{\gamma_D}, \mathbf{k})$ is the four-momentum of dark photon. The benchmark Lagrangian of that simplified ALP portal scenario can be written as follows

$$\begin{aligned} \mathcal{L} \supset & \mathcal{L}_{\text{dark axion portal}} + \bar{\chi}(\gamma^\mu i \partial_\mu - g_D \gamma^\mu A'_\mu + m_\chi)\chi \\ & + \sum_{l=e,\mu} i g_l^p a \bar{l} \gamma_5 l, \end{aligned} \quad (30)$$

where we consider only the pseudoscalar coupling of the ALP to the leptons g_l^p . The numerical calculations reveal that the scalar coupling to leptons $\mathcal{L} \supset \sum_{l=e,\mu} g_l^s a \bar{l} l$ yields the similar contribution to the signal events if we set universal coupling as $g_l^s = g_l^p$.

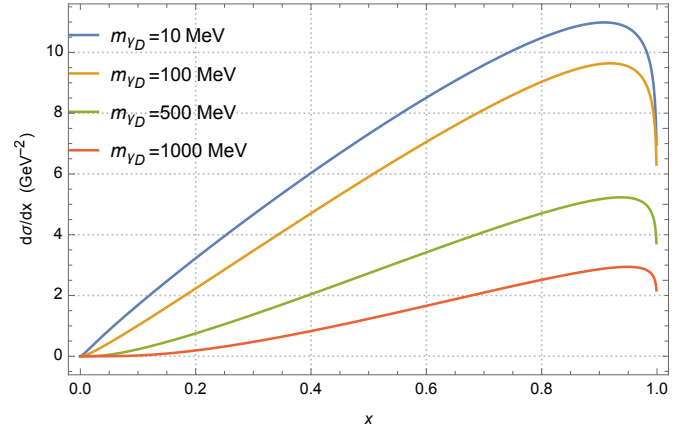


FIG. 13. The differential cross-section of dark photon production at NA64e as a function of fraction energy $x = E_{\gamma_D} / E_l$ for the ALP-leptophilic scenario and for various masses m_{γ_D} . We set $m_a = 10$ keV, $g_l^p = 1$, $g_{a\gamma\gamma_D} = 1$ GeV $^{-1}$ and $E_e = 100$ GeV.

To calculate the cross-section of the process (29) we use the equivalent photon approximation [59, 94, 106], that implies the factorization of $2 \rightarrow 3$ rate into the product of photon flux and $2 \rightarrow 2$ cross-section of the Compton-like process $l(p)\gamma(q) \rightarrow l(p')\gamma_D(k)$

$$\frac{d\sigma_{lZ \rightarrow lZ\gamma_D}}{d(pk)d(k\mathcal{P}_i)} \simeq \frac{\alpha\chi}{\pi(p'\mathcal{P}_i)} \cdot \left. \frac{d\sigma_{l\gamma \rightarrow l\gamma_D}}{d(pk)} \right|_{t=t_{min}}, \quad (31)$$

where χ is the effective photon flux from nucleus [59], in (31) we assume that the photon virtuality t has its minimum t_{min} when \mathbf{q} is collinear with $\mathbf{k} - \mathbf{p}$. We define auxiliary Mandelstam variables and regarding identity as follows

$$\tilde{u} = (p - k)^2 - m_l^2, \quad \tilde{s} = (p' + k)^2 - m_l^2, \quad (32)$$

$$t_2 = (p - p')^2, \quad \tilde{s} + \tilde{u} + t_2 \simeq m_{\gamma_D}^2, \quad (33)$$

then one can easily obtain the following expression for the differential cross-section in the Lorentz invariant notations [59, 94, 106]

$$\frac{d\sigma_{2 \rightarrow 2}}{d(pk)} \simeq \frac{1}{8\pi\tilde{s}^2} \cdot |\overline{\mathcal{M}_{2 \rightarrow 2}}|^2. \quad (34)$$

Let us calculate now the amplitude of the relevant $2 \rightarrow 2$ sub-process

$$\mathcal{M}_{2 \rightarrow 2} = g_l^p g_{a\gamma\gamma_D} \frac{\bar{u}(p')\gamma_5 u(p)}{t_2 - m_a^2} \epsilon_\mu(q) \epsilon_\nu^*(k) \epsilon^{\mu\nu qk}, \quad (35)$$

where $\epsilon^{\mu\nu qk} = q_\lambda k_\rho \epsilon^{\mu\nu\lambda\rho}$. As the result of averaging over polarizations one gets the following expression for the amplitude squared

$$\begin{aligned} |\overline{\mathcal{M}_{2 \rightarrow 2}}|^2 &= \frac{1}{4} \sum_{\text{pol}} |\mathcal{M}_{2 \rightarrow 2}|^2 \\ &= -\frac{1}{4} \frac{(g_l^p)^2 g_{a\gamma\gamma_D}^2}{(t_2 - m_a^2)^2} t_2 \lambda(t_2, 0, m_{\gamma_D}^2), \end{aligned} \quad (36)$$

where $\lambda(x, y, z) = x^2 + y^2 + z^2 - 2xy - 2xz - 2yz$ is the kinematical triangle Källén function. These calculations are performed by exploiting the state-of-the-art FeynCalc package [101] of Wolfram Mathematica [102].

It is worth noting that longitudinal term $k_\mu k_\nu / m_{\gamma_D}^2$ in the dark photon polarization tensor $\sum_i \epsilon_\mu^{*i}(k) \epsilon_\nu^i(k)$ does not contribute to the matrix element squared due to the current conservation. We label the energy fraction of γ_D boson by $x = E_{\gamma_D}/E_l$ and the angle between \mathbf{k} and \mathbf{p} by θ_{γ_D} . Let us introduce the auxiliary function U as follows

$$U \equiv -\tilde{u} \simeq E_l^2 \theta_{\gamma_D}^2 x + m_{\gamma_D}^2 (1 - x)/x + m_l^2 x, \quad (37)$$

in (37) we keep only leading terms in $m_{\gamma_D}^2/E_l^2$, m_l^2/E_l^2 , $m_l^2/E_l'^2$ and $\theta_{\gamma_D}^2$. In the latter approach one has

$$t_{min} \simeq U^2 / (4E_l^2 (1 - x)^2), \quad (38)$$

$$\tilde{s} \simeq U / (1 - x), \quad t_2 \simeq -xU / (1 - x) + m_{\gamma_D}^2. \quad (39)$$

Finally, we obtain the expression for the double differential cross-section

$$\frac{d\sigma_{2 \rightarrow 3}}{dx d\cos\theta_{\gamma_D}} \simeq \frac{\alpha\chi}{\pi(1-x)} \cdot E_l^2 x \beta_{\gamma_D} \cdot \frac{d\sigma_{2 \rightarrow 2}}{d(pk)}, \quad (40)$$

where $\beta_{\gamma_D} = (1 - m_{\gamma_D}^2 / (xE_l)^2)^{1/2}$ is the velocity of dark photon in the laboratory frame. The explicit analytical expression for the effective photon flux χ is given in the Ref. [59] for the case of elastic form-factor $G_{el}(t)$ that is proportional to $\propto Z^2$. An inelastic form factor $G_{inel}(t) \propto Z$ and for the heavy target nuclei $Z \propto \mathcal{O}(100)$, so that one can safely ignore it in the calculation below.

The resulted cross-section can be rewritten as

$$\begin{aligned} \frac{d\sigma_{2 \rightarrow 3}}{dx d\cos\theta_{\gamma_D}} &\simeq \frac{\alpha\chi}{32\pi^2} E_l^2 \beta_{\gamma_D} (g_l^p)^2 g_{a\gamma\gamma_D}^2 \\ &\times \frac{x^3 [xU - m_{\gamma_D}^2 (1 - x)]}{[xU - (1 - x)(m_{\gamma_D}^2 - m_a^2)]^2}. \end{aligned} \quad (41)$$

As an example, in Fig. (13) we show the differential cross-sections of the process $eZ \rightarrow eZ\gamma_D$ as a function of x for NA64e experiment and the benchmark ALP-leptophilic setup (30) with $m_a = 10$ keV. The WW approximation for the leptophilic cross-section implies that the photon flux χ from nucleus is the function of x and θ_{γ_D} , so that it is fairly accurate approach for the exact tree level cross-section (for detail, see e. g. Ref. [59] and references therein).

In Fig. 15 of Sec. VIII the 90 % *C.L.* sensitivity curves of the fixed target experiments are shown for the combination of couplings $|g_{a\gamma\gamma_D} g_l^p|$. To plot these curves we put $N_{sign} > 2.3$, implying null result for the DM detection and background free case.

VIII. SUMMARY AND DISCUSSION

In the present paper in addition to ALP contribution to lepton EDM we have calculated the novel limits on the combination of *CP*-even and *CP*-odd couplings of neutron with ALPs from the current constraints on neutron EDM by taking into account its anomalous magnetic moment. The regarding contribution to neutron EDM is associated with a light scalar/pseudoscalar boson exchange at 1-loop level. This contribution is proportional to $\sim \bar{\theta}$ of QCD parameter of *CP*-violation [79, 80]. In addition we have considered the possible implication of dark axion portal couplings to the EDM of SM fermions. In particular, we have calculated at the 1-loop level the EDM, that can be induced by the three specific model-independent interactions: (i) *CP*-odd Yukawa-like couplings of ALP with fermions, (ii) *CP*-even interaction of SM fermions and light vector boson, and (iii) *CP*-even dark axion/ALP portal coupling. Such Barr-Zee type diagrams have an ultraviolet (UV) logarithmic divergences, which can be calculated by using \overline{MS} regularization scheme and removed by exploiting the local counter-terms of EDM type. We briefly discuss the regarding renormalization procedure in Appendix B.

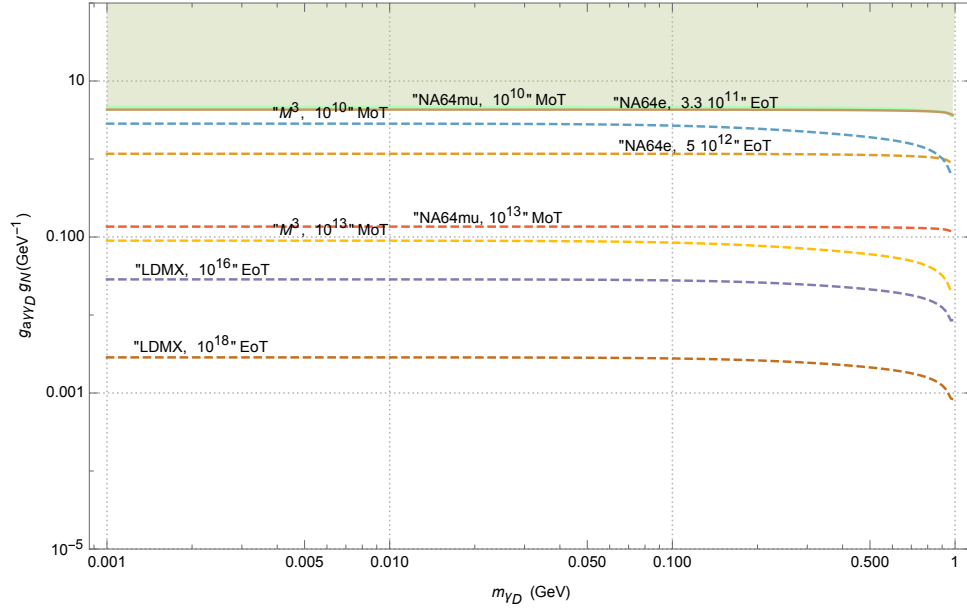


FIG. 14. Bounds on combination of couplings ALPs with gauge fields $g_{a\gamma\gamma_D}$ and ALP couplings with nucleons $g^s = g^p = g_N$ for hadrophilic channel from current and proposal statistics of the experiments NA64e, NA64 μ , LDMX and M³. We set here $\text{Br}(\gamma_D \rightarrow \chi\bar{\chi}) \simeq 1$ and $m_a = 10$ keV.

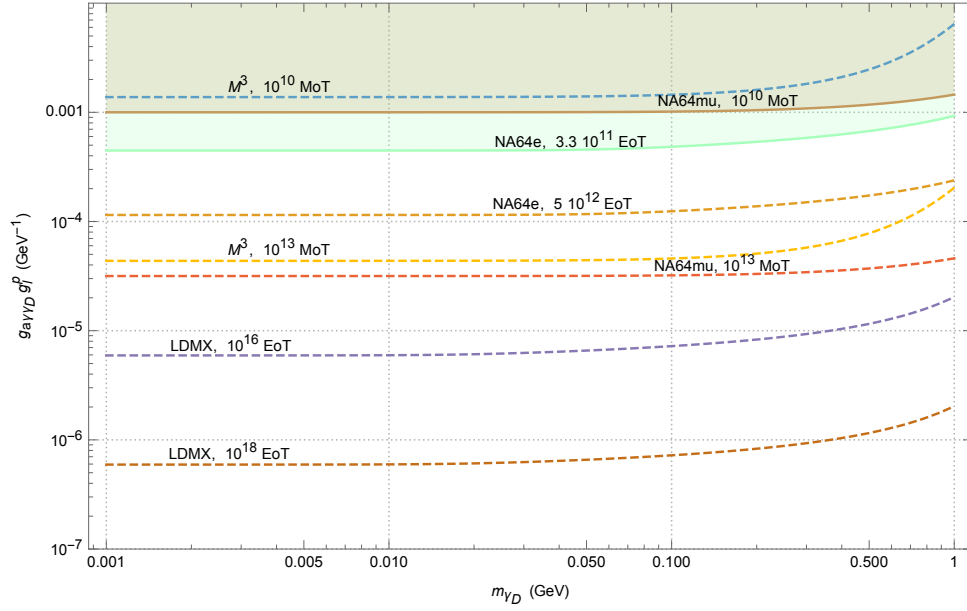


FIG. 15. Bounds for the combination of ALP couplings with leptons g_l^p and with gauge fields $g_{a\gamma\gamma_D}$ for the leptophilic scenario from current and proposal statistics of the NA64e, NA64 μ , LDMX and M³ experiments. We set here $m_a = 10$ keV and $\text{Br}(\gamma_D \rightarrow \chi\bar{\chi}) \simeq 1$.

We have also discussed in detail the probing the dark ALP portal scenario through the dark photon decaying predominantly to the DM particles, $\text{Br}(\gamma_D \rightarrow \chi\bar{\chi}) \simeq 1$. In the present paper we refer the relevant benchmark model as minimal dark ALP portal scenario (see bounds

for $g_{a\gamma\gamma_D}$ coupling in Fig. 9). This scenario implies that dark photon is $U_D(1)$ gauge field and serves the mediator between DM and SM particles through the dark axion portal. In this scenario we imply that $m_a \ll m_{\gamma_D}$, therefore the visible decay $a \rightarrow \gamma\gamma_D$ is kinematically for-

bidden.

We have studied in detail the missing energy signatures for the projected and existed lepton fixed target facilities, such as NA64e, LDMX, NA64 μ and M^3 . In particular, by using state-of-the-art **CalcHEP** package we calculated the $a\gamma_D$ pair production cross-sections in the processes $lZ \rightarrow lZa\gamma_D$ followed by the invisible dark photon decay into DM particles $\gamma_D \rightarrow \chi\bar{\chi}$ for the specific fixed target facility. We have calculated the sensitivity curves for these experiments using the null result for DM detection for the existed and planned statistics of leptons accumulated on target, such called invisible mode.

We have discussed in detail the expected reach of the NA64e experiment to probe the dark photon emission via the missing energy process of vector meson production $eZ \rightarrow eZJ/\psi$ followed by invisible decay $J/\psi \rightarrow a\gamma_D (\rightarrow \chi\bar{\chi})$. We have shown that latter signal process dominates over the bremsstrahlung $a\gamma_D$ pair emission in the reaction $eZ \rightarrow eZ\gamma^* (\rightarrow a\gamma_D)$ at NA64e. Thus expected reach of NA64e from $J/\psi \rightarrow a\gamma_D$ can rule out the projected bounds from the off-shell photon emission for EOT $\simeq 5 \times 10^{12}$.

We have recasted the BaBar monophoton data $e^+e^- \rightarrow a\gamma\gamma_D$ to derive constraints on the dark ALP portal coupling, implying that the dark photon decays mainly to the DM fermion pair. We have shown that the existed BaBar bounds rule out the current NA64e constraints for EOT $\simeq 3 \times 10^{11}$.

We have considered the modifications of the minimal dark ALP portal scenario by including two benchmark Lagrangians in the model: hadron- and lepton-specific couplings which imply ALP Yukawa-like interaction mainly with hadrons and leptons respectively. For both hadron- and lepton-specific scenarios we have calculated the cross-sections of dark photon production $lZ \rightarrow lZ\gamma_D$ by using WW approximation. Calculation in WW approximation is in a reasonable agreement with exact tree-level calculation performed with **CalcHEP**.

The calculations reveal the differences between both hadrophilic and leptophilic cross-sections of dark photon production. First, the ALP-hadrophilic cross-section is relatively small since it scales to the first power of nucleon/atomic number $\propto A$. Contrary, the ALP-leptophilic rate of γ_D production is enhanced due to the factor $\propto Z^2$. Second, the hadrophilic cross-section is sensitive of the cut on the angle of dark photon emission θ_{γ_D} . Large θ_{γ_D} leads to the inelastic scattering that is associated with significant transfer momentum to nucleon. So that, in present analysis we conservatively set the upper benchmark value $\theta_{\gamma_D} \lesssim \theta_{\gamma_D}^{max} \simeq 0.1$ rad in order to get rid of the inelastic interaction of ALP with nucleus matter. On the other hand, the leptophilic cross-section $d\sigma_{2 \rightarrow 3}/dx$ depends weakly on $\theta_{\gamma_D}^{max}$, since $d\sigma_{2 \rightarrow 3}/d\theta_{\gamma_D}$ has a very narrow peak at the typical angles of dark photon emission $\theta_{\gamma_D} \simeq m_l/E_l \ll 1$.

Moreover, we want to note that total cross-section for the hadrophilic scenario is suppressed relative to leptophilic one. The suppression factor is estimated to be of

the order of $\sim 10^{-7} \div 10^{-5}$. Thus the resulted hadrophilic constraints are weaker than leptophilic bounds for the same number of leptons accumulated on target. That difference can be found in both Fig. 14 and Fig. 15 where the bounds on the combination of couplings for the hadrophilic and leptophilic scenarios are depicted respectively. In the framework of considered benchmark scenarios, the most stringent constraints on the couplings are expected from the projected experiment LDMX.

In the future we plan to consider also the possible benchmark dark ALP portal signatures along with both ALP portal and vector portal scenarios.

ACKNOWLEDGMENTS

We would like to thank N. Arefyeva, R. Capdevilla, A. Celentano, X. Chu, P. Crivelli, S. Demidov, D. Forbes, S. Gninenko, D. Gorbunov, Y. Kahn, M. Kirsanov, N. Krasnikov, G. Krnjaic, L. Molina Bueno, A. Pimikov, J. Pradler, A. Pukhov, P. Schuster, H. Sieber and F. Tkachov¹ for very helpful discussions and correspondences.

This work was funded by BMBF (Germany) “Verbunddark photon projekt 05P2021 (ErUM-FSP T01) - Run 3 von ALICE am LHC: Perturbative Berechnungen von Wirkungsquerschnitten für ALICE” (Förderkennzeichen: 05P21VTCAA), by ANID PIA/APOYO AFB180002 (Chile), by FONDECYT (Chile) under Grant No. 1191103, and by ANID-Millennium Program-ICN2019_044 (Chile). This research was supported by TSU and TPU development programs. The work of A.S.Z. is supported by Grant of AYSS JINR (22-302-02). The work of D.V.K on description of the dark matter missing energy signatures of NA64e and regarding exclusion limits for the minimal dark axion portal scenario is supported by the Russian Science Foundation RSF grant 21-12-00379.

Appendix A: Analytic form of loop integral

Here we present analytic form for loop integrals (6) and (8) which are used for fermion EDM calculation:

$$g_1(y) = 1 - y^2 \log y - \frac{y(y^2 - 2)}{2\sqrt{y^2 - 4}} \times \left(\arctan \left(\frac{y^2 - 2}{y\sqrt{y^2 - 4}} \right) - \arctan \left(\frac{y}{\sqrt{y^2 - 4}} \right) \right), \quad (\text{A1})$$

¹ Deceased

$$g_2(y) = k_n \left\{ \frac{3}{2} - y^2 + (y^2 - 3)y^2 \log y + \frac{\sqrt{y^2 - 4}}{2} \times \right. \\ \left. (y^2 - 2)y \left(\arctan \frac{y}{\sqrt{y^2 - 4}} + \arctan \frac{2 - y^2}{y\sqrt{y^2 - 4}} \right) \right. \\ \left. + \frac{y^3}{2} \sqrt{y^2 - 4} \left(\arctan \frac{y}{\sqrt{y^2 - 4}} - \arctan \frac{2 - y^2}{y\sqrt{y^2 - 4}} \right) \right\}. \quad (\text{A2})$$

Appendix B: Lepton EDM induced by the Barr-Zee diagrams with lepton-dark photon-axion loop

Here we consider details of calculation of the correction to the lepton EDM induced by Barr-Zee diagrams with lepton-dark photon-axion loop. In order to remove the logarithmic divergence containing in the Barr-Zee diagrams we add the local counter-term, which is induced by the following Lagrangian

$$\mathcal{L}_{\text{ct}} = g_{\text{ct}}(\mu) F_{\mu\nu} \bar{l} i \sigma^{\mu\nu} \gamma^5 l, \quad (\text{B1})$$

where $g_{\text{ct}}(\mu)$ is the coupling constant depending on renormalization scale μ . In particular, we choose $g_{\text{ct}}(\mu)$ as

$$g_{\text{ct}}(\mu) = g \left[\frac{1}{\bar{\epsilon}} - \gamma \log \frac{m_l^2}{\mu^2} \right], \quad (\text{B2})$$

where m_l is the lepton mass, g and γ are the parameters, which will be fixed to drop divergence in the Barr-Zee diagrams and guarantee scale independence of the result for lepton EDM. Here, $\bar{\epsilon}$ is the pole in the $\overline{\text{MS}}$ renormalization scheme:

$$\frac{1}{\bar{\epsilon}} = \frac{1}{\epsilon} + \Gamma'(1) - \log(4\pi) \quad (\text{B3})$$

Therefore, the contribution of the counter-term to the lepton EDM is

$$d_l^{\text{ct}} = -2g \left[\frac{1}{\bar{\epsilon}} + \gamma \log \frac{m_l^2}{\mu^2} \right] \quad (\text{B4})$$

The contribution of the Barr-Zee diagrams to the lepton EDM reads

$$d_l^{\text{BZ}} = \frac{G}{8\pi^2} \left[\frac{1}{\bar{\epsilon}} - \int_0^1 d^3\alpha \log \frac{\Delta}{\mu^2} \right], \quad (\text{B5})$$

where $G = g_{a\gamma\gamma_D} g_s e\epsilon$ is the effective coupling, which is the product of three respective couplings between photon, dark photon, axion, and leptons (see e. g. Eq. (10) for detail),

$$\Delta = m_{A'}^2 \alpha_1 + m_a^2 \alpha_2 + m_l^2 \alpha_3^2, \quad (\text{B6})$$

where

$$\int_0^1 d^3\alpha \equiv \int_0^1 d\alpha_1 \int_0^1 d\alpha_2 \int_0^1 d\alpha_3 \delta\left(1 - \sum_{i=1}^3 \alpha_i\right). \quad (\text{B7})$$

Result for the lepton EDM can be written as

$$d_l = d_l^{\text{BZ}} + d_l^{\text{ct}} = \frac{2}{\bar{\epsilon}} \left[\frac{G}{16\pi^2} - g \right] \\ - 2 \log \frac{m_l^2}{\mu^2} \left[\frac{G}{16\pi^2} - g\gamma \right] - \frac{G}{4\pi^2} \int_0^1 d^3\alpha \log \frac{\Delta}{\mu^2}. \quad (\text{B8})$$

From Eq. (B8) follows that the couplings g and γ must fixed as

$$g = \frac{G}{16\pi^2}, \quad \gamma = 1. \quad (\text{B9})$$

Finally, one gets

$$d_l = -\frac{G}{4\pi^2} \int_0^1 d^3\alpha \log \frac{\Delta}{\mu^2}. \quad (\text{B10})$$

After integration over two Feynman parameters we have

$$d_l = -\frac{G}{4\pi^2} \left[-\frac{1}{2} + \frac{I(m_{A'}^2) - I(m_a^2)}{m_{A'}^2 - m_a^2} \right], \quad (\text{B11})$$

where

$$I(m^2) = \int_0^1 dx \left[m^2(1-x) + m_l^2 x^2 \right] \\ \times \log \frac{m^2(1-x) + m_l^2 x^2}{\mu^2} \quad (\text{B12})$$

Next, it is interesting to consider a few limiting cases:

(1) $m_l = 0$

$$d_l = -\frac{G}{4\pi^2} \left[-1 + \frac{I_0(m_{A'}^2) - I_0(m_a^2)}{m_{A'}^2 - m_a^2} \right], \quad (\text{B13})$$

where

$$I_0(m^2) = m^2(1-x) \log \frac{m^2}{\mu^2}. \quad (\text{B14})$$

(2) $m_l = 0, m_{A'} = m_a = m$

$$d_l = -\frac{G}{8\pi^2} \left[-1 + \log \frac{m^2}{\mu^2} \right] \quad (\text{B15})$$

[1] R. D. Peccei and H. R. Quinn, Phys. Rev. D **16**, 1791 (1977).

[2] L. Di Luzio, M. Giannotti, E. Nardi, and L. Visinelli, Phys. Rept. **870**, 1 (2020), arXiv:2003.01100 [hep-ph].

- [3] T. Aoyama *et al.*, Phys. Rept. **887**, 1 (2020), arXiv:2006.04822 [hep-ph].
- [4] A. E. Dorokhov, A. E. Radzhabov, and A. S. Zhevlakov, JETP Lett. **100**, 133 (2014), arXiv:1406.1019 [hep-ph].
- [5] C. Boehm and P. Fayet, Nucl. Phys. B **683**, 219 (2004), arXiv:hep-ph/0305261.
- [6] M. J. Dolan, F. Kahlhoefer, C. McCabe, and K. Schmidt-Hoberg, JHEP **03**, 171 (2015), [Erratum: JHEP **07**, 103 (2015)], arXiv:1412.5174 [hep-ph].
- [7] Y. Hochberg, E. Kuflik, R. McGehee, H. Murayama, and K. Schutz, Phys. Rev. D **98**, 115031 (2018), arXiv:1806.10139 [hep-ph].
- [8] C. Han, M. L. López-Ibáñez, A. Melis, O. Vives, and J. M. Yang, Phys. Rev. D **103**, 035028 (2021), arXiv:2007.08834 [hep-ph].
- [9] H. Davoudiasl, R. Marcarelli, and E. T. Neil, (2021), arXiv:2112.04513 [hep-ph].
- [10] S. N. Gninenko and N. V. Krasnikov, (2022), arXiv:2202.04410 [hep-ph].
- [11] M. Bauer, M. Neubert, S. Renner, M. Schnubel, and A. Thamm, JHEP **04**, 063 (2021), arXiv:2012.12272 [hep-ph].
- [12] K. Choi, S. H. Im, and C. Sub Shin, Ann. Rev. Nucl. Part. Sci. **71**, 225 (2021), arXiv:2012.05029 [hep-ph].
- [13] R. R. Dusaev, D. V. Kirpichnikov, and M. M. Kirsanov, Phys. Rev. D **102**, 055018 (2020), arXiv:2004.04469 [hep-ph].
- [14] D. Banerjee *et al.* (NA64), Phys. Rev. Lett. **125**, 081801 (2020), arXiv:2005.02710 [hep-ex].
- [15] H. Ishida, S. Matsuzaki, and Y. Shigekami, Phys. Rev. D **103**, 095022 (2021), arXiv:2006.02725 [hep-ph].
- [16] Y. Sakaki and D. Ueda, Phys. Rev. D **103**, 035024 (2021), arXiv:2009.13790 [hep-ph].
- [17] V. Brdar, B. Dutta, W. Jang, D. Kim, I. M. Shoemaker, Z. Tabrizi, A. Thompson, and J. Yu, Phys. Rev. Lett. **126**, 201801 (2021), arXiv:2011.07054 [hep-ph].
- [18] D. Salnikov, P. Satunin, D. V. Kirpichnikov, and M. Fitkevich, JHEP **03**, 143 (2021), arXiv:2011.12871 [hep-ph].
- [19] Z. Bogorad, A. Hook, Y. Kahn, and Y. Soreq, Phys. Rev. Lett. **123**, 021801 (2019), arXiv:1902.01418 [hep-ph].
- [20] Y. Kahn, B. Giaccone, A. Lunin, A. Netepenko, R. Pilipenko, and M. Wentzel, Proc. SPIE Int. Soc. Opt. Eng. **12016**, 29 (2022).
- [21] L. Darmé, F. Giacchino, E. Nardi, and M. Raggi, JHEP **06**, 009 (2021), arXiv:2012.07894 [hep-ph].
- [22] P. S. B. Dev, D. Kim, K. Sinha, and Y. Zhang, Phys. Rev. D **104**, 035037 (2021), arXiv:2101.08781 [hep-ph].
- [23] H. Abramowicz *et al.*, Eur. Phys. J. ST **230**, 2445 (2021), arXiv:2102.02032 [hep-ex].
- [24] J.-F. Fortin, H.-K. Guo, S. P. Harris, D. Kim, K. Sinha, and C. Sun, Int. J. Mod. Phys. D **30**, 2130002 (2021), arXiv:2102.12503 [hep-ph].
- [25] K. Asai, S. Iwamoto, Y. Sakaki, and D. Ueda, JHEP **09**, 183 (2021), arXiv:2105.13768 [hep-ph].
- [26] R. Balkin, M. W. Krasny, T. Ma, B. R. Safdi, and Y. Soreq, (2021), 10.1002/andp.202100222, arXiv:2105.15072 [hep-ph].
- [27] N. Blinov, E. Kowalczyk, and M. Wynne, JHEP **02**, 036 (2022), arXiv:2112.09814 [hep-ph].
- [28] I. Larin *et al.* (PrimEx), Phys. Rev. Lett. **106**, 162303 (2011), arXiv:1009.1681 [nucl-ex].
- [29] S. N. Gninenko, N. V. Krasnikov, M. M. Kirsanov, and D. V. Kirpichnikov, Phys. Rev. D **94**, 095025 (2016), arXiv:1604.08432 [hep-ph].
- [30] D. Banerjee *et al.* (NA64), Phys. Rev. Lett. **118**, 011802 (2017), arXiv:1610.02988 [hep-ex].
- [31] S. N. Gninenko, D. V. Kirpichnikov, M. M. Kirsanov, and N. V. Krasnikov, Phys. Lett. B **782**, 406 (2018), arXiv:1712.05706 [hep-ph].
- [32] S. N. Gninenko, D. V. Kirpichnikov, M. M. Kirsanov, and N. V. Krasnikov, Phys. Lett. B **796**, 117 (2019), arXiv:1903.07899 [hep-ph].
- [33] D. Banerjee *et al.*, Phys. Rev. Lett. **123**, 121801 (2019), arXiv:1906.00176 [hep-ex].
- [34] Y. M. Andreev *et al.*, Phys. Rev. D **104**, L091701 (2021), arXiv:2108.04195 [hep-ex].
- [35] Y. M. Andreev *et al.* (NA64), Phys. Rev. Lett. **126**, 211802 (2021), arXiv:2102.01885 [hep-ex].
- [36] N. Blinov, G. Krnjaic, and D. Tucker, Phys. Rev. D **103**, 035030 (2021), arXiv:2010.03577 [hep-ph].
- [37] T. D. Beattie *et al.*, Nucl. Instrum. Meth. A **896**, 24 (2018), arXiv:1801.03088 [physics.ins-det].
- [38] R. Essig *et al.*, in *Community Summer Study 2013: Snowmass on the Mississippi* (2013) arXiv:1311.0029 [hep-ph].
- [39] G. Arcadi, A. Djouadi, and M. Raidal, Phys. Rept. **842**, 1 (2020), arXiv:1903.03616 [hep-ph].
- [40] F. Fortuna, P. Roig, and J. Wudka, JHEP **02**, 223 (2021), arXiv:2008.10609 [hep-ph].
- [41] A. J. Buras, A. Crivellin, F. Kirk, C. A. Manzari, and M. Montull, JHEP **06**, 068 (2021), arXiv:2104.07680 [hep-ph].
- [42] A. Kachanovich, S. Kovalenko, S. Kuleshov, V. E. Lyubovitskij, and A. S. Zhevlakov, Phys. Rev. D **105**, 075004 (2022), arXiv:2111.12522 [hep-ph].
- [43] M. Escudero, N. Rius, and V. Sanz, JHEP **02**, 045 (2017), arXiv:1606.01258 [hep-ph].
- [44] Y. Nomura and J. Thaler, Phys. Rev. D **79**, 075008 (2009), arXiv:0810.5397 [hep-ph].
- [45] K. Kaneta, H.-S. Lee, and S. Yun, Phys. Rev. Lett. **118**, 101802 (2017), arXiv:1611.01466 [hep-ph].
- [46] K. Kaneta, H.-S. Lee, and S. Yun, Phys. Rev. D **95**, 115032 (2017), arXiv:1704.07542 [hep-ph].
- [47] J. C. Gutiérrez, B. J. Kavanagh, N. Castelló-Mor, F. J. Casas, J. M. Diego, E. Martínez-González, and R. V. Cortabitarte, (2021), arXiv:2112.11387 [hep-ph].
- [48] P. deNiverville, H.-S. Lee, and M.-S. Seo, Phys. Rev. D **98**, 115011 (2018), arXiv:1806.00757 [hep-ph].
- [49] P. deNiverville and H.-S. Lee, Phys. Rev. D **100**, 055017 (2019), arXiv:1904.13061 [hep-ph].
- [50] S. Alekhin *et al.*, Rept. Prog. Phys. **79**, 124201 (2016), arXiv:1504.04855 [hep-ph].
- [51] J. L. Feng *et al.*, (2022), arXiv:2203.05090 [hep-ex].
- [52] P. deNiverville, H.-S. Lee, and Y.-M. Lee, Phys. Rev. D **103**, 075006 (2021), arXiv:2011.03276 [hep-ph].
- [53] V. Domcke, K. Schmitz, and T. You, (2021), arXiv:2108.11295 [hep-ph].
- [54] S.-F. Ge, X.-D. Ma, and P. Pasquini, Eur. Phys. J. C **81**, 787 (2021), arXiv:2104.03276 [hep-ph].
- [55] D. V. Kirpichnikov, V. E. Lyubovitskij, and A. S. Zhevlakov, Phys. Rev. D **102**, 095024 (2020), arXiv:2002.07496 [hep-ph].
- [56] D. V. Kirpichnikov, V. E. Lyubovitskij, and A. S. Zhevlakov, Particles **3**, 719 (2020), arXiv:2004.13656 [hep-ph].
- [57] S. N. Gninenko, N. V. Krasnikov, and V. A. Matveev,

- Phys. Rev. D **91**, 095015 (2015), arXiv:1412.1400 [hep-ph].
- [58] S. N. Gninenko and N. V. Krasnikov, Phys. Lett. B **783**, 24 (2018), arXiv:1801.10448 [hep-ph].
- [59] D. V. Kirpichnikov, H. Sieber, L. M. Bueno, P. Crivelli, and M. M. Kirsanov, Phys. Rev. D **104**, 076012 (2021), arXiv:2107.13297 [hep-ph].
- [60] H. Sieber, D. Banerjee, P. Crivelli, E. Depero, S. N. Gninenko, D. V. Kirpichnikov, M. M. Kirsanov, V. Poliakov, and L. Molina Bueno, Phys. Rev. D **105**, 052006 (2022), arXiv:2110.15111 [hep-ex].
- [61] J. Mans (LDMX), EPJ Web Conf. **142**, 01020 (2017).
- [62] A. Berlin, N. Blinov, G. Krnjaic, P. Schuster, and N. Toro, Phys. Rev. D **99**, 075001 (2019), arXiv:1807.01730 [hep-ph].
- [63] T. Åkesson *et al.* (LDMX), (2018), arXiv:1808.05219 [hep-ex].
- [64] A. M. Ankowski, A. Friedland, S. W. Li, O. Moreno, P. Schuster, N. Toro, and N. Tran, Phys. Rev. D **101**, 053004 (2020), arXiv:1912.06140 [hep-ph].
- [65] P. Schuster, N. Toro, and K. Zhou, Phys. Rev. D **105**, 035036 (2022), arXiv:2112.02104 [hep-ph].
- [66] T. Åkesson *et al.*, in *2022 Snowmass Summer Study* (2022) arXiv:2203.08192 [hep-ex].
- [67] Y. Kahn, G. Krnjaic, N. Tran, and A. Whitbeck, JHEP **09**, 153 (2018), arXiv:1804.03144 [hep-ph].
- [68] R. Capdevilla, D. Curtin, Y. Kahn, and G. Krnjaic, (2021), arXiv:2112.08377 [hep-ph].
- [69] B. Holdom, Phys. Lett. B **166**, 196 (1986).
- [70] J. F. Gunion, H. E. Haber, G. L. Kane, and S. Dawson, *The Higgs Hunter's Guide*, Vol. 80 (2000).
- [71] A. Djouadi, Phys. Rept. **459**, 1 (2008), arXiv:hep-ph/0503173.
- [72] G. C. Branco, P. M. Ferreira, L. Lavoura, M. N. Rebelo, M. Sher, and J. P. Silva, Phys. Rept. **516**, 1 (2012), arXiv:1106.0034 [hep-ph].
- [73] E. J. Chun and T. Mondal, JHEP **07**, 044 (2021), arXiv:2104.03701 [hep-ph].
- [74] V. A. Dzuba, V. V. Flambaum, I. B. Samsonov, and Y. V. Stadnik, Phys. Rev. D **98**, 035048 (2018), arXiv:1805.01234 [physics.atom-ph].
- [75] V. Flambaum, S. Lambert, and M. Pospelov, Phys. Rev. D **80**, 105021 (2009), arXiv:0902.3217 [hep-ph].
- [76] H. Yan, G. A. Sun, S. M. Peng, H. Guo, B. Q. Liu, M. Peng, and H. Zheng, Eur. Phys. J. C **79**, 971 (2019).
- [77] C. A. J. O'Hare and E. Vitagliano, Phys. Rev. D **102**, 115026 (2020), arXiv:2010.03889 [hep-ph].
- [78] P. A. Zyla *et al.* (Particle Data Group), PTEP **2020**, 083C01 (2020).
- [79] A. S. Zhevlakov and V. E. Lyubovitskij, Phys. Rev. D **101**, 115041 (2020), arXiv:2003.12217 [hep-ph].
- [80] R. J. Crewther, P. Di Vecchia, G. Veneziano, and E. Witten, Phys. Lett. B **88**, 123 (1979), [Erratum: Phys.Lett.B 91, 487 (1980)].
- [81] A. S. Zhevlakov, M. Gorchtein, A. N. Hiller Blin, T. Gutsche, and V. E. Lyubovitskij, Phys. Rev. D **99**, 031703 (2019), arXiv:1812.00171 [hep-ph].
- [82] A. S. Zhevlakov, T. Gutsche, and V. E. Lyubovitskij, Phys. Rev. D **99**, 115004 (2019), arXiv:1904.08154 [hep-ph].
- [83] T. Gutsche, A. N. Hiller Blin, S. Kovalenko, S. Kuleshov, V. E. Lyubovitskij, M. J. Vicente Vacas, and A. Zhevlakov, Phys. Rev. D **95**, 036022 (2017), arXiv:1612.02276 [hep-ph].
- [84] D. E. Maisson and L. V. Skripnikov, Phys. Rev. A **105**, 032813 (2022), arXiv:2201.12574 [physics.atom-ph].
- [85] D. V. Kirpichnikov, V. E. Lyubovitskij, and A. S. Zhevlakov, In preparation.
- [86] A. Belyaev, N. D. Christensen, and A. Pukhov, Comput. Phys. Commun. **184**, 1729 (2013), arXiv:1207.6082 [hep-ph].
- [87] V. M. Budnev, I. F. Ginzburg, G. V. Meledin, and V. G. Serbo, Phys. Rept. **15**, 181 (1975).
- [88] R. Engel, A. Schiller, and V. G. Serbo, Z. Phys. C **71**, 651 (1996), arXiv:hep-ph/9511262.
- [89] M. I. Vysotsky and E. Zhemchugov, Phys. Usp. **62**, 910 (2019), arXiv:1806.07238 [hep-ph].
- [90] M. Bondi, A. Celentano, R. R. Dusaev, D. V. Kirpichnikov, M. M. Kirsanov, N. V. Krasnikov, L. Marsicano, and D. Shchukin, Comput. Phys. Commun. **269**, 108129 (2021), arXiv:2101.12192 [hep-ph].
- [91] X. Chu, J. Pradler, and L. Semmelrock, Phys. Rev. D **99**, 015040 (2019), arXiv:1811.04095 [hep-ph].
- [92] C.-Y. Chen, M. Pospelov, and Y.-M. Zhong, Phys. Rev. D **95**, 115005 (2017), arXiv:1701.07437 [hep-ph].
- [93] S. N. Gninenko, D. V. Kirpichnikov, and N. V. Krasnikov, Phys. Rev. D **100**, 035003 (2019), arXiv:1810.06856 [hep-ph].
- [94] J. D. Bjorken, R. Essig, P. Schuster, and N. Toro, Phys. Rev. D **80**, 075018 (2009), arXiv:0906.0580 [hep-ph].
- [95] Y.-S. Tsai, Phys. Rev. D **34**, 1326 (1986).
- [96] B. Abi *et al.* (Muon g-2), Phys. Rev. Lett. **126**, 141801 (2021), arXiv:2104.03281 [hep-ex].
- [97] R. H. Parker, C. Yu, W. Zhong, B. Estey, and H. Müller, Science **360**, 191 (2018), arXiv:1812.04130 [physics.atom-ph].
- [98] P. A. Zyla *et al.* (Particle Data Group), PTEP **2020**, 083C01 (2020).
- [99] I. R. Blokland, A. Czarnecki, and K. Melnikov, Phys. Rev. Lett. **88**, 071803 (2002), arXiv:hep-ph/0112117.
- [100] A. Mangoni, *Hadronic decays of the J/ψ meson*, Ph.D. thesis, Università Di Perugia (2020), arXiv:2002.09675 [hep-ph].
- [101] V. Shtabovenko, R. Mertig, and F. Orellana, Comput. Phys. Commun. **207**, 432 (2016), arXiv:1601.01167 [hep-ph].
- [102] W. R. Inc., “Mathematica, Version 13.0.0,” Champaign, IL, 2021.
- [103] N. Arefyeva, S. Gninenko, D. Gorbunov, and D. Kirpichnikov, (2022), arXiv:2204.03984 [hep-ph].
- [104] B. Döbrich, J. Jaeckel, F. Kahlhoefer, A. Ringwald, and K. Schmidt-Hoberg, JHEP **02**, 018 (2016), arXiv:1512.03069 [hep-ph].
- [105] E. Byckling and K. Kajantie, *Particle Kinematics* (University of Jyväskylä, Jyväskylä, Finland, 1971).
- [106] Y.-S. Liu and G. A. Miller, Phys. Rev. D **96**, 016004 (2017), arXiv:1705.01633 [hep-ph].